JOURNAL OF GEOPHYSICAL RESEARCH, VOL. 114, D06210, doi:10.1029/2008JD010680, 2009

Aging of black carbon in outflow from anthropogenic sources using a mixing state resolved model: Model development and evaluation

N. Oshima,[1,2] M. Koike,[1] Y. Zhang,[3] Y. Kondo,[4] N. Moteki,[4] N. Takegawa,[4] and Y. Miyazaki[5]

Received 29 June 2008; revised 26 November 2008; accepted 5 January 2009; published 27 March 2009.

[1] The mixing state of black carbon (BC) aerosols, namely, the degree to which BC particles are coated with other aerosol components, has been recognized as important for evaluating aerosol radiative forcing. In order to resolve the BC mixing state explicitly in model simulations, a two-dimensional aerosol representation, in which aerosols are given for individual particle diameters and BC mass fractions, is introduced. This representation was incorporated into an aerosol module, the Model of Aerosol Dynamics, Reaction, Ionization, and Dissolution (MADRID), and a new box model, MADRID-BC, was developed. MADRID-BC can accurately simulate changes in the entire BC mixing state resulting from condensation/evaporation processes. Aircraft observations conducted in March 2004 show that the mass fraction of thickly coated BC particles increased in air horizontally transported out from an urban area in Japan over the ocean. MADRID-BC generally reproduces this feature well when observed bulk aerosol concentrations are used as constraints. The model simulations in this particular case show that for particles with BC core diameters of 100–200 nm, the particle diameters, including both core and coating materials, had already increased by a factor of 1.6 on average when they left the source region and by as large as a factor of 1.9 of the BC core diameters after their transport over the ocean for a half day. The model simulations also show that 58% of the total condensed mass was partitioned onto BC-free particles during transport, indicating their importance for the BC mixing state. Although the model simulations are applied to a limited number of the observations in this study, they clearly show the time evolution of the coating thicknesses of BC-containing particles, which is necessary for calculating aerosol optical properties and cloud condensation nuclei activities.

Citation: Oshima, N., M. Koike, Y. Zhang, Y. Kondo, N. Moteki, N. Takegawa, and Y. Miyazaki (2009), Aging of black carbon in outflow from anthropogenic sources using a mixing state resolved model: Model development and evaluation, *J. Geophys. Res.*, *114*, D06210, doi:10.1029/2008JD010680.

1. Introduction

[2] Atmospheric aerosols modify the global radiation budget directly through scattering and absorption of solar radiation and indirectly through modification of the microphysical properties of clouds. Most aerosol components scatter solar radiation; however, black carbon (BC) aerosols (e.g., soot) efficiently absorb it. The absorption leads to heating of the atmosphere and cooling of the surface below, resulting in increases in the regional vertical stability of the atmosphere, therefore likely reducing convective activity and cloud formation [*Hansen et al.*, 1997; *Ackerman et al.*, 2000; *Koren et al.*, 2004]. These light-absorbing effects possibly lead to modifications of the large-scale atmospheric circulation and hydrological cycle [*Ramanathan et al.*, 2001a; *Menon et al.*, 2002]. In contrast, the reduction of cloud cover by atmospheric heating can increase the solar radiation reaching the surface below, resulting in heating of the surface [*Hansen et al.*, 1997]. Consequently, the impacts of BC on the climate system are complex and involve various feedback mechanisms [*Jacobson*, 2002a]. Because of the significance of these various mechanisms, the role of BC in the climate system has been recognized as particularly important [*Hansen et al.*, 1997; *Jacobson*, 2002a; *Wang*, 2004; *Intergovernmental Panel on Climate Change* (IPCC), 2007].

[3] BC particles are emitted into the atmosphere by incomplete combustion of fossil fuels (diesel and coal),

[1]Department of Earth and Planetary Science, Graduate School of Science, University of Tokyo, Tokyo, Japan.
[2]Now at Research Center for Advanced Science and Technology, University of Tokyo, Tokyo, Japan.
[3]Department of Marine, Earth, and Atmospheric Sciences, North Carolina State University, Raleigh, North Carolina, USA.
[4]Research Center for Advanced Science and Technology, University of Tokyo, Tokyo, Japan.
[5]Institute of Low Temperature Science, Hokkaido University, Sapporo, Japan.

0148-0227/09/2008JD010680$09.00

biomass, and biofuels. The anthropogenic emissions of BC are greatest in Asian countries [*Streets et al.*, 2003; *Bond et al.*, 2004], such as China, India, and Korea, where BC emissions are dominated by coal-based thermal power plants [*Prasad et al.*, 2006], with BC mixing with dust particles especially in the Asian region [*Prasad and Singh*, 2007; *Bhattacharjee et al.*, 2007]. Previous studies have shown that the anthropogenic pollutants emitted over east Asia are either transported within the planetary boundary layer (PBL) or uplifted to the free troposphere (FT) by convection and warm conveyor belts followed by efficient horizontal transport on a regional-to-hemispheric scale [*Bey et al.*, 2001; *Koike et al.*, 2003; *Miyazaki et al.*, 2003; *Liu et al.*, 2003; *Oshima et al.*, 2004]. Among these pollutants, several studies have focused on the spatial distributions and transport processes of BC particles emitted from Asia (mainly China and India) within the PBL [*Ramanathan et al.*, 2001b; *Uno et al.*, 2003] and in the FT [*Clarke et al.*, 2004; *Park et al.*, 2005]. These BC particles are considered to have significant impacts on the radiation budget and therefore the climate system on regional-to-hemispheric scales.

[4] The mixing state of BC, namely, the degree to which BC particles are coated with other aerosol components, can affect the impact of BC particles on the radiation in two ways [*Stier et al.*, 2006]. First, BC particles freshly emitted into the atmosphere are generally in the form of bare particles externally mixed with other particles and therefore in a hydrophobic state [*Weingartner et al.*, 1997; *Sakurai et al.*, 2003]. They gradually become internally mixed through condensation, coagulation, and/or photochemical oxidation processes in the atmosphere (aging processes). They eventually become hydrophilic, when they are coated with sufficient water-soluble compounds, such as ammonium sulfate ($(NH_4)_2SO_4$), and are able to serve as cloud condensation nuclei (CCN). The CCN activity of a BC-containing particle primarily depends on the dry particle diameter and mass fraction of soluble material in the particle [e.g., *Seinfeld and Pandis*, 2006]. Therefore, aging processes increase the wet scavenging efficiency of BC and consequently reduce the amount of BC transported from the PBL to the FT. Second, coatings on BC particles with nonabsorbing compounds enhance the BC absorption efficiency of solar radiation [*Bond et al.*, 2006]. This enhancement depends on the BC core diameter and shell diameter, the latter defined as the particle diameter including both the BC core and coating materials [*Bohren and Huffman*, 1983; *Bond et al.*, 2006]. *Jacobson* [2001] showed that coatings on BC particles enhance their impact on the direct radiative forcing. Consequently, to accurately estimate aerosol optical properties and CCN activities of BC-containing particles, information on both the size distribution of BC cores and mass concentrations of their coating materials (particle shell diameters), or equivalently, the distribution of BC-containing particles as a function of both the BC core diameter and BC mass fraction, must be known. This information is referred to as "entire BC mixing state" in this paper.

[5] A number of previous modeling studies have evaluated the radiative effects of aerosols including BC; however, the entire BC mixing state was not accurately treated in most of these studies except some advanced modeling studies [e.g., *Jacobson*, 2001; *Jacobson*, 2002b]. *Jacobson* [2001] used a global model that treated condensation and coagulation processes with 18 discrete aerosol size distributions, each with 17 size bins. Eight of these size distributions contained BC and three of these BC-containing distributions treated fixed ranges of BC mass fraction in each bin (i.e., 0–5%, 5–20%, and >20% in volume fractional coatings) and the others treated variable BC mass fraction ranges in each distribution for each size, which allowed for the representation of several degrees of coatings of BC particles. While the results of the predicted BC mixing states were consistent with ambient observations [*Jacobson*, 2001], such observations did not provide quantitative information on coating thicknesses (volume fractions) of individual BC-containing particles.

[6] In recent years, advanced observation techniques using laser-induced incandescence (single-particle soot photometer, SP2) have been developed, enabling us to obtain some quantitative information on the mixing states of BC-containing particles [*Baumgardner et al.*, 2004; *Schwarz et al.*, 2006; *Gao et al.*, 2007; *Moteki and Kondo*, 2007]. Although the number of measurements is still limited, they show that BC-containing particles with different shell diameters but with the same BC core diameter coexist in the atmosphere [*Schwarz et al.*, 2008] and that the coating thicknesses of BC particles change through BC aging processes [*Moteki et al.*, 2007]. These recent observations provide opportunities to test our current understanding of BC aging processes through comparisons with model simulations.

[7] In light of recent observations, we introduced a new aerosol representation into an aerosol module, the Model of Aerosol Dynamics, Reaction, Ionization, and Dissolution (MADRID) [*Zhang et al.*, 2004], following the method developed by *Jacobson* [2001], to explicitly simulate the BC mixing state. In this representation, aerosol mass and number are given for individual particle diameters and BC mass fractions, so that the coexistence of BC particles with different shell diameters but with the same BC core diameter can be tracked for all ranges of BC core diameter. This new MADRID module was incorporated into a box model that couples with gas-phase chemistry. The resulting newly developed box model is referred to as the MADRID-BC model hereafter. MADRID-BC simulates the condensation/evaporation process using a dynamic gas/particle mass transfer approach in order to accurately represent the growth of individual particles. To validate the BC mixing state treatments in MADRID-BC and understand the evolution of the entire BC mixing state, MADRID-BC was applied to a case in which the BC aging process was observed in air transported out from an urban area in Japan (Nagoya city) with aircraft measurements using an SP2 experiment [*Moteki et al.*, 2007]. A comparison of the model simulation results with the observations is presented here along with a full picture of the predicted changes in the entire BC mixing state.

2. Model Description

2.1. BC Mixing State Resolved Aerosol Representation

[8] A two-dimensional (2-D) aerosol representation, which enables the resolution of the BC mixing state explicitly, was introduced in this study following the method

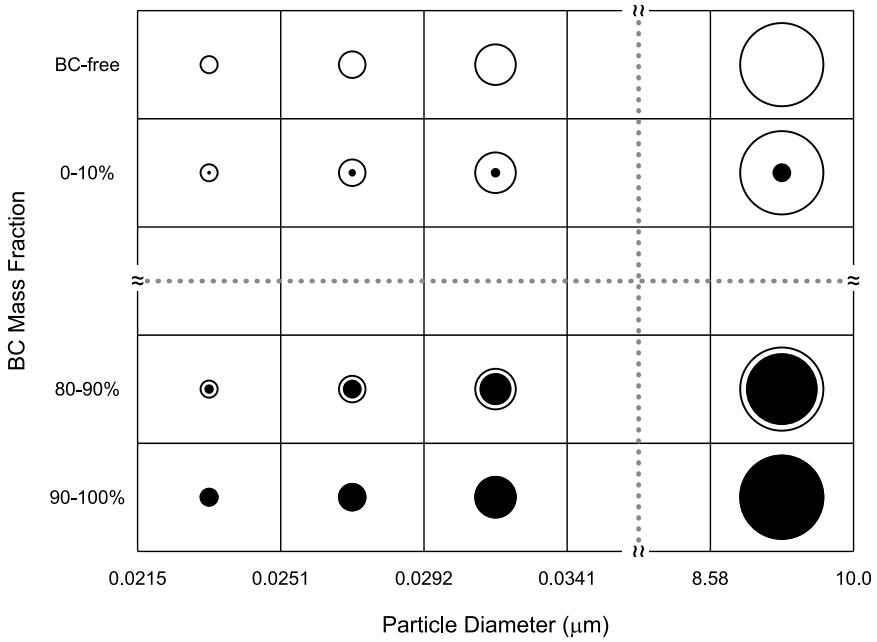

Figure 1. Schematic diagram of the two-dimensional (2-D) aerosol representation adopted in the MADRID-BC box model developed in this study. In this representation, the particle number and aerosol mass of individual compounds are given for each grid cell, which consists of the dry particle diameter and dry BC mass fraction, where BC mass fraction is defined as the ratio of the mass of bare BC to that of the particle. Particles with smaller BC mass fractions correspond to those having greater coating amounts on BC. In this study, 40 size sections, ranging from 0.0215 μm to 10 μm, are employed, and BC mass fractions are divided into 10 even sections between 0 and 100%. In addition to BC-containing particles, BC-free particles are also represented. The chemical compositions of coating materials can vary in each grid cell.

of *Jacobson* [2001]. In this representation, aerosol mass and number are given for individual particle diameters and BC mass fractions as illustrated in Figure 1. This representation can be viewed as a 2-D aerosol representation; particles having the same diameter but with different BC mass fractions can be treated separately. BC particles with smaller BC mass fractions correspond to those having greater coating amounts. The distributions of aerosol size and BC mass fraction are divided into discrete bins by dry particle diameter and by dry BC mass fraction, respectively. The number of sections of particle size and BC mass fraction can be chosen flexibly. In this study, 40 size sections, ranging from 0.0215 μm to 10 μm, were employed, and BC mass fractions were divided into ten even sections between 0 and 100%. In addition to BC-containing particles, externally mixed "BC-free" particles, which do not contain BC, were treated separately. As shown in section 4, these BC-free particles play an important role in the partitioning of condensable materials onto particles and therefore affect the BC mixing state. Furthermore, consideration of BC-free particles is essential in calculating aerosol optical properties (N. Oshima et al., Aging of black carbon in outflow from anthropogenic sources using a mixing state resolved model: 2. Aerosol optical properties and cloud condensation nuclei activities, submitted to *Journal of Geophysical Research*, 2008). Species considered in this study include sulfate (SO_4^{2-}), ammonium (NH_4^+), nitrate (NO_3^-), sodium (Na^+), chloride (Cl^-), aerosol water, BC, and organic matter (OM). In the 2-D aerosol representation, the chemical compositions of coating materials can vary with both particle size and BC mass fraction, so that differences in chemical composition among the grid cells can be expressed. The particle number and mass of individual aerosol compositions are calculated for each grid cell. Dry and wet particle diameters can be derived from the number and mass of aerosol particles in each grid cell.

[9] Freshly emitted BC particles from the tail pipe of a diesel engine truck are reported to have, in general, only a small amount of coating materials [*Sakurai et al.*, 2003; *Park et al.*, 2004; *Wehner et al.*, 2004], although there is little quantitative information regarding the BC mixing state upon emission. Because of the uncertainties in the mixing states of freshly emitted BC particles, we assume all freshly emitted BC particles have a 100% BC mass fraction and put them in the 90–100% BC mass fraction grid cell in the present model simulations. Note that the possible diameter range of bare BC particles (100% BC mass fraction) upon emission is 0.023–9.3 μm in the simulations. In Appendix A1, we show results from a sensitivity simulation in which the influences of emissions of partly coated BC particles on the BC mixing state in the atmosphere are evaluated. When BC particles in a given grid cell are coated with other aerosol materials, such as $(NH_4)_2SO_4$, owing to condensation, their particle diameters increase and BC mass fractions decrease. Eventually, the particles in the grid cell grow into another grid cell with a larger particle size and/or a smaller BC mass fraction. We note here that when aerosols are represented only by particle diameter, as used in most current aerosol models (i.e., a 1-D representation), freshly emitted BC particles are forced to be mixed with preexisting particles

in given size sections, resulting in thick coatings that may not be realistic. In contrast, the 2-D aerosol representation allows the fresh BC particles to remain as thinly coated BC particles, even when thickly coated BC particles already exist in given size sections, because particles having different BC mass fractions can coexist with any given particle diameter.

[10] Transfer of particle number and mass between grid cells due to their growth or shrinkage is simulated on the basis of the moving center approach [*Jacobson*, 1997] that was implemented as a 1-D approach in MADRID [*Zhang et al.*, 2004]. In this study, we expanded the 1-D moving center approach in MADRID to a 2-D aerosol representation so that the transfer of particles can be simulated simultaneously in both directions, namely, particle diameter and BC mass fraction. This approach allows us to track mass and number concentrations within the 2-D aerosol representation. MADRID-BC also allows use of the "full-moving" approach, which is useful for accurately tracking the Lagrangian growth of particles due to condensation/evaporation processes [*Jacobson*, 1999].

[11] A number of previous studies have treated aerosol particles as spherical, on the basis of the idea that although BC particles may have complex nonspherical morphology upon emission, they tend to transform into a near-spherical morphology owing to aging processes in the atmosphere [*Jacobson*, 2000; *Riemer et al.*, 2003; *Bond et al.*, 2006; *Stier et al.*, 2007; *Schwarz et al.*, 2008]. In this study, the spherical assumption of aerosols was used.

2.2. Physical and Chemical Processes in MADRID-BC

[12] The 2-D aerosol representation described above was incorporated into the MADRID aerosol module, and a new MADRID-BC box model, in which the MADRID aerosol module was coupled with a gas-phase chemistry module, was developed. A detailed description of MADRID was given by *Zhang et al.* [2004]. The MADRID-BC box model was constructed as a stand-alone model so that it can simulate the time evolution of BC mixing state due to chemical production/loss of aerosol compounds in the atmosphere. Although most physical and chemical processes treated in the MADRID module are utilized in MADRID-BC, some new features have been introduced into MADRID-BC in order to accurately simulate the BC mixing state. The physical and chemical processes used in this study are described below, although the original MADRID offers several options.

[13] The most important process for BC aging is condensation/evaporation due to mass transfer between gas and particle phases. To simulate accurately the growth of individual particles, a dynamic (kinetic) nonequilibrium approach developed by *Meng et al.* [1998] was adopted in this study, although bulk equilibrium approaches were adopted for fine particles in the original MADRID module. The following growth law is used in MADRID-BC to simulate the mass flux of species i onto a single spherical particle [*Meng et al.*, 1998],

$$J_i = \frac{dm_i}{dt} = 2\pi D_p D_i \frac{C_{\infty,i} - C_{s,i}}{\frac{2\lambda_m}{\alpha_i D_p} + 1}, \quad (1)$$

where m_i is the single particle mass of species i, D_p is the particle diameter, D_i is the molecular diffusivity of species i in air, $C_{\infty,i}$ and $C_{s,i}$ are the concentrations in the bulk gas phase and those at the particle surface, respectively, λ_m is the air mean free path, and α_i is the accommodation coefficient for species i on the atmospheric aerosol. Because limited information is available regarding α_i in the atmosphere, α_i values used in previous modeling studies vary by a few orders of magnitudes [*Wexler et al.*, 1994]. In this study, α_i of 0.1 was assumed for all species, following *Zhang et al.* [2004]. Particle surface vapor concentrations $C_{s,i}$ for volatile inorganic compounds, namely ammonia (NH_3), nitric acid (HNO_3), and hydrogen chloride (HCl), were estimated using the aerosol thermodynamic module ISORROPIA [*Nenes et al.*, 1998, 1999]. For sulfuric acid, we assumed the particle surface vapor concentration is zero for all particles because of its extremely low vapor pressure [*Meng et al.*, 1998]. An exception is water, which was assumed to be in local instantaneous equilibrium between the gas and aerosol phases [*Wexler et al.*, 1994; *Meng et al.*, 1998]. Condensation/evaporation involving secondary organic aerosols (SOAs) and their precursors is not included in the dynamic approach in MADRID-BC but was treated separately in this study, as described in section 4. In MADRID-BC, the mass flux of species i given by equation (1) is calculated for each grid cell (i.e., each size and each BC mass fraction; see Figure 1) simultaneously using each $C_{s,i}$ values estimated by ISORROPIA and common gas-phase bulk concentrations at every small time step. Note that this time step for gas-aerosol mass transfer calculations is set to be one second in this study so as to satisfy the numerical stability.

[14] Coagulation is not included in MADRID-BC, following the original MADRID. Coagulation may play an important role for BC aging, particularly near emission sources, where aerosol number concentrations are very high. *Jacobson* [2002b] showed that even with moderate loading of particulates, coagulation alone could change the mixing state of aerosols to some degree within 12 h. Consequently, the exclusion of coagulation could result in an underestimation of the BC aging rate in our simulation. However, we focused on BC aging processes in air transported out from a city over distances of a few hundred kilometers in this study, as described in section 3. In this case, coagulation was considered to play a relatively minor role as compared with condensation because the timescale of coagulation is longer than that of condensation. In fact, coagulation was not included in some other aerosol modeling studies at urban scales [e.g., *Zhang et al.*, 2004; *Fast et al.*, 2006]. A simple evaluation of the effects of coagulation on BC mixing state in our application (section 4) is presented in Appendix A2. The BC aging process due to photochemical oxidation is also not included in MADRID-BC. *Croft et al.* [2005] indicated that the contribution of oxidation to the BC aging process may be small, and oxidation processes were not included in many aerosol models [e.g., *Riemer et al.*, 2004].

[15] Other processes treated in MADRID-BC are briefly described below. MADRID-BC uses the gas-phase chemistry of the Carbon-Bond Mechanism Version IV (CBM-IV) photochemical mechanism [*Gery et al.*, 1989], which con-

tains 92 chemical species and 117 chemical reactions. Heterogeneous reactions on the surface of particles are included in MADRID-BC. In this formulation, the first-order heterogeneous reaction rate constants are calculated at individual grid cells, on the basis of the approach of *Zhang et al.* [1994], *Zhang and Carmichael* [1999], and *Jacob* [2000]. Although the original MADRID includes nucleation processes [*Zhang et al.*, 2004], they were not used in this study because they are subject to large uncertainties [*Zhang and Jacobson*, 2005; *Zhang et al.*, 2005]. The dilution of air, dry and wet deposition, and aqueous-phase chemistry in cloud particles are not included in MADRID-BC. Meteorological conditions (e.g., air density, pressure, temperature, relative humidity, and cloud/rain information) are kept constant throughout each simulation in MADRID-BC. Photolysis rates of chemical reactions are also provided in MADRID-BC by adopting the approach used in the Community Multiscale Air Quality (CMAQ) model [*Byun and Ching*, 1999].

3. Observed Features of BC Mixing States

[16] During the Pacific Exploration of Asian Continental Emission phase C (PEACE-C) aircraft mission, which was conducted over the western Pacific around Japan between 22 and 27 March 2004, evidence of the evolution of the coating thickness of BC particles in urban plumes was observed [*Moteki et al.*, 2007]. In the present study, we applied the MADRID-BC box model to this case to validate the model simulations and examine changes in the entire BC mixing state in detail. In this section, the aircraft measurements and observed features are described.

3.1. Aircraft Measurements

[17] The PEACE-C aircraft mission was conducted within the framework of an atmospheric chemistry project by the Earth Observation Research Center (EORC) of the Japan Aerospace Exploration Agency (JAXA). In total, five flights were conducted using a Gulfstream II (G-II) aircraft. A detailed description of the measurements during the PEACE-C mission was given by *Moteki et al.* [2007]. Here, we briefly describe the instrumentation and observations.

[18] The size distribution of volume equivalent diameters of BC particles excluding their coating materials was measured by an SP2 instrument using the laser-induced incandescence technique [*Baumgardner et al.*, 2004; *Schwarz et al.*, 2006; *Moteki and Kondo*, 2007]. In this paper, this diameter is denoted as the BC core diameter, D_{BC}, while the particle diameter including coating materials is denoted as the shell diameter, D_P. From the laser scattering signal detected by the SP2 instrument, some information on the coating condition of BC particles can be obtained. During the PEACE-C aircraft measurements, thinly and thickly coated BC particles were discriminated [*Moteki et al.*, 2007]. These two types of aerosols generally correspond to BC particles that have D_P/D_{BC} ratios smaller or greater than a particular threshold D_P/D_{BC} value. There is an uncertainty in the threshold D_P/D_{BC} value and it was estimated to be between 1.5 and 2.0 during PEACE-C. These BC discriminations were made for particles with BC core diameters (D_{BC}) between 155 and 330 nm. The mass fraction of thickly coated BC particles, $f_{thick}(D_{BC})$, is defined for individual BC core diameters, D_{BC}, as follows,

$$f_{thick}(D_{BC}) = \frac{[BC_{thick}(D_{BC})]}{[BC_{thick}(D_{BC})] + [BC_{thin}(D_{BC})]}, \quad (2)$$

where $[BC_{thick}(D_{BC})]$ and $[BC_{thin}(D_{BC})]$ are the total BC mass concentrations of thickly and thinly coated BC particles for the given BC core diameter (D_{BC}), respectively. Given a BC core diameter, the number of BC particles observed can be converted into BC mass. In addition to BC particle size distributions, particle sizes of BC-free particles were also obtained for volume equivalent diameters between 300 and 800 nm, although they could have contained BC particles with BC core diameters smaller than 150 nm, which are not detected by the SP2 instrument.

[19] The total mass concentrations of BC particles were independently measured by a particle soot absorption photometer with a heated inlet (HI-PSAP), assuming a mass absorption coefficient of 8.9 $m^2\ g^{-1}$ [*Kondo et al.*, 2006]. The uncertainty in this value was estimated to be smaller than 10% [*Kondo et al.*, 2006]. Because the SP2 measurement did not cover the entire BC size range, HI-PSAP data were used for total BC mass concentrations in this study. The SP2 data were utilized for the BC core size distribution and the mass fraction of thickly coated BC particles, $f_{thick}(D_{BC})$.

[20] Bulk mass concentrations of water-soluble inorganic ions and water-soluble organic carbon (WSOC) were measured by a particle-into-liquid sampler with ion chromatography analysis (PILS-IC) and a PILS with a total carbon analyzer (PILS-WSOC) technique, respectively [*Miyazaki et al.*, 2006]. A portion of these compounds is considered to have been internally mixed with BC particles, and the remainder is assumed to have existed as BC-free particles, although this information cannot be derived from the bulk measurements. In this study, SO_4^{2-} values were used as non-sea-salt SO_4^{2-} ($nssSO_4^{2-}$) values to maximize the number of data points to be compared with model simulations, because SO_4^{2-} values agree to within 10% with $nssSO_4^{2-}$ when $nssSO_4^{2-}$ amounts are calculated using an empirical relationship between SO_4^{2-} and Na^+ in seawater. Total sulfur compounds (SO_x) are defined as the sum of sulfur dioxide (SO_2) and SO_4^{2-}. Primary and secondary organic aerosol (POA and SOA) mass concentrations were estimated independently from the observed BC and WSOC concentrations, respectively, using the POA-BC and SOA-WSOC relationships observed in the Tokyo urban area, Japan (see Appendix A3). Total organic aerosol (OA) mass concentration was simply derived from the sum of POA and SOA mass concentrations.

3.2. General Observed Features During Flight 5

[21] During PEACE-C flight 5 conducted over the Pacific off the coast of Japan on 27 March under cloud-free conditions, clear changes in the fraction of thickly coated BC particles were observed as a function of photochemical age in the urban plume transported within the PBL from Japan [*Moteki et al.*, 2007]. We focused on these data and made detailed comparisons between model simulations and observations, as described in section 4.

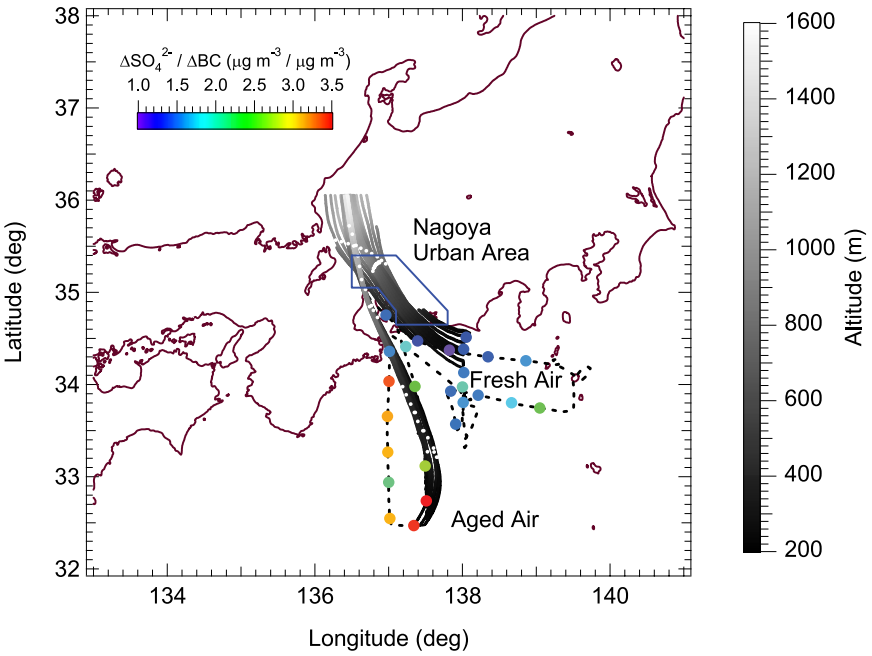

Figure 2. Flight tracks of the aircraft observations during PEACE-C flight 5 (black dashed lines) and 2-day back trajectories of "fresh" and "aged" air parcels (thick lines). These two air parcel groups are defined by their transport time over the ocean after leaving the coastline of Japan. The transport time was shortest (2 h) and longest (13 h) in "fresh" and "aged" air parcels, respectively. The altitudes of the trajectories are shown in gray scale. White dots on the trajectories denote the locations of air parcels 6 and 12 h prior to measurement. Colored circles denote the bulk $\Delta SO_4^{2-}/\Delta BC$ ratios observed along the flight track. The region outlined by the blue line denotes the Nagoya urban area defined in this study.

[22] Kinematic back trajectories of air parcels sampled onboard the aircraft in the PBL during flight 5 were calculated using the method described by *Tomikawa and Sato* [2005], and meteorological fields were calculated using the Fifth-Generation Pennsylvania State University/National Center for Atmospheric Research (NCAR) Mesoscale Model (MM5) [*Grell et al.*, 1995]. In Figure 2, 2-day back trajectories are shown for two air parcel groups, which were transported from over the Nagoya urban area, Japan (the area enclosed within the blue solid line in Figure 2 as defined in this study). Within air parcels sampled by the aircraft in the PBL, these two groups had the shortest (2 h) and longest (13 h) transport times over the ocean after leaving the coastline of Japan, and they are referred to as "fresh" and "aged" air, respectively, hereafter. The trajectories of the air parcels sampled in the PBL show that most of the air parcels had been transported horizontally from over the Nagoya urban area by northerly winds within the PBL. These air parcels had likely been influenced by anthropogenic emission sources over the Nagoya urban area, because their altitudes were below 1.5 km when they were over that area. In urban areas in Japan, the major source of BC is considered to be exhaust from diesel engines [*Kondo et al.*, 2006]. Ratios of various primary compounds, such as BC-to-carbon monoxide (CO) ratios, were similar within the air parcels, suggesting that they were influenced by the same types of emission sources over the Nagoya urban area and were likely not influenced by wet removal during transport (see Appendix A4). In fact, MM5 simulations, cloud images from the Geostationary Operational Environmental Satellite (GOES-9), and the Rader-Automated Meteorological Data Acquisition System (Rader-AMeDAS) precipitation analysis show that the air parcels had very little chance to encounter clouds or precipitation. These results suggest that the data set obtained in the PBL during flight 5 is suitable to study the Lagrangian time evolution of BC mixing states within these air parcels.

[23] In order to evaluate the amount of secondary aerosol production (or loss), which can lead to growth (or shrinkage) of coatings of BC particles, and to exclude apparent changes in concentration due to dilution with background air, a normalized ratio, $\Delta X/\Delta BC$, was calculated for various species X, where ΔX and ΔBC are differences between observed and background concentrations of X and BC, respectively, in individual air parcels. In this study, the background concentrations of BC, CO, SO_4^{2-}, and NH_4^+ were chosen to be 0, 150, 0.10, and 0.20 ppbv, respectively, which were the minimum values observed during flight 5. For other chemical species, background concentrations were assumed to have been zero. We note that when only dilution by mixing with background air takes place, the $\Delta X/\Delta BC$ value does not change and is equal to the value in air leaving the source region.

[24] Concentrations of various gaseous and aerosol species as well as their normalized ratios, $\Delta X/\Delta BC$, in "fresh" and "aged" air parcels are shown in Table 1. As shown in Table 1, although the CO and SO_x concentrations were lower in "aged" air as compared with those in "fresh" air, the normalized ratios change little, indicating that the observed changes were primarily due to dilution with background air (see Appendix A4). On the other hand, the normalized ratios of SO_4^{2-} and WSOC increased by a factor

Table 1. Observed Concentrations of Various Chemical Species, Their Normalized Ratios to BC, and Mass Fractions of Thickly Coated BC Particles in Air Parcels Sampled During PEACE-C Flight 5

	Concentrations[a]		ΔX/ΔBC Ratios[b]	
Species	Fresh Air	Aged Air	Fresh Air	Aged Air
CO, ppbv	269	196	85.2	81.6
BC, μg m^{-3}	1.40	0.569		
SO_x, ppbv	2.35	0.966	1.61	1.52
SO_2, ppbv	1.80	0.383	1.29	0.673
SO_4^{2-}, μg m^{-3}	2.19	2.34	1.32	3.51
NH_4^+, μg m^{-3}	1.31	0.764	0.843	1.12
NO_3^-, μg m^{-3}	1.94	0.126	1.39	0.221
WSOC,[c] μgC m^{-3}	1.20	1.14	0.861	1.99
$f_{thick}(D_{BC})$[d]	0.343	0.618		

[a]Mean concentration in "fresh" and "aged" air parcels.
[b]Normalized ratios, ΔX/ΔBC, for various species X, where ΔX and ΔBC are differences between observed and background concentrations of X and BC, respectively. These values are given using the units of X and BC shown in the first column.
[c]Mass concentration of water-soluble organic carbon (WSOC).
[d]Mass fraction of thickly coated BC particles, $f_{thick}(D_{BC})$, defined by equation (2), for BC core diameters (D_{BC}) of 155–185 nm.

of more than two, as also pointed out by *Moteki et al.* [2007] using X/BC mass ratios. The observed increase in ΔSO_4^{2-}/ΔBC ratios during transport was quite likely due to photochemical production of SO_4^{2-}. Corresponding to the shortest and longest transport times in "fresh" and "aged" air parcels, the smallest and greatest values of ΔSO_4^{2-}/ΔBC ratios were observed in "fresh" and "aged" air, respectively (Figure 2). Similarly, the observed increase in ΔWSOC/ΔBC ratios suggests significant production of SOA, because WSOC is generally considered to be produced through SOA formation [*Kondo et al.*, 2007].

[25] In Figure 3a, observed values of the mass fraction of thickly coated BC particles, $f_{thick}(D_{BC})$, which is defined by equation (2), are shown as a function of the ΔSO_4^{2-}/ΔBC ratios for D_{BC} of 155–185 nm. Note that the $f_{thick}(D_{BC})$ value does not change by dilution with background air when BC particles do not exist in background air. *Moteki et al.* [2007] showed that $f_{thick}(D_{BC})$ values increase with increasing photochemical age. Because of the increasing trend in ΔSO_4^{2-}/ΔBC ratios with the photochemical age of air (not shown), the results shown in Figure 3a are considered to be another expression of the time evolution of $f_{thick}(D_{BC})$ values. As shown in Figure 3a, observed $f_{thick}(D_{BC})$ values increase continuously from 0.34 ("fresh" air) to 0.62 ("aged" air) as ΔSO_4^{2-}/ΔBC ratios increase from 1.3 to 3.5 (Table 1). This result clearly shows that the fraction of thickly coated BC particles increased as the photochemical production of SO_4^{2-} proceeded during transport. Because of the Lagrangian nature of these air parcels described above, this increasing tendency can be viewed as a Lagrangian time evolution of the BC mixing state from "fresh" to "aged" air parcels during transport over the ocean.

4. Predicted Evolution of BC Mixing States

[26] In order to simulate the entire BC mixing state in air sampled during flight 5, simulations for two consecutive regimes were performed using the MADRID-BC box model. The simulation in the first regime is for the source region where emissions of BC and POA particles were continuously introduced, and concurrent coatings due to condensation were calculated for both preexisting and newly emitted particles. The simulation in the second regime, which follows the first regime simulation, is for the outflow region over the ocean, where the coating process without the emissions took place. In both regimes, the photochemical production of condensable compounds, such as sulfuric acid, from their precursor gases were calculated. The results obtained from the end of the first and the second regime simulations correspond to observations in "fresh" and "aged" air, respectively. The time evolution of the BC mixing state obtained from the second regime simulation is compared with those of observations as a function of ΔSO_4^{2-}/ΔBC ratio, which was a minimum and maximum

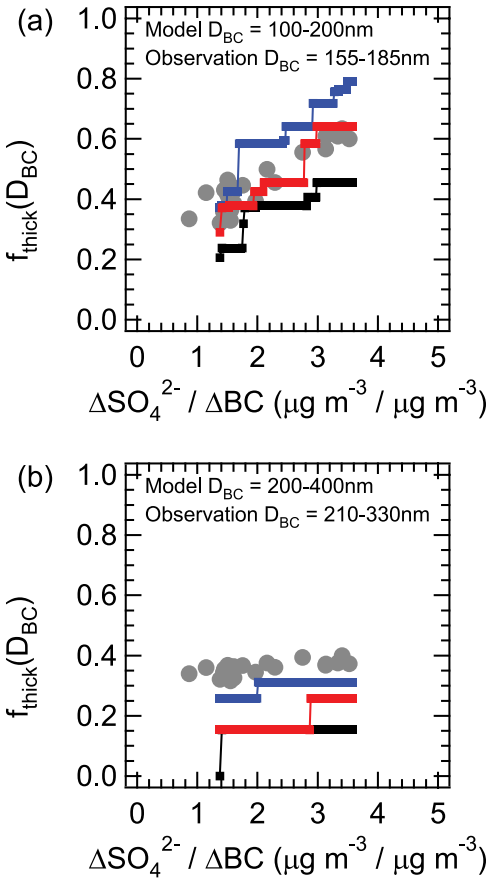

Figure 3. Observed and model-predicted mass fractions of thickly coated BC particles, $f_{thick}(D_{BC})$, defined by equation (2), as a function of the bulk ΔSO_4^{2-}/ΔBC ratio. Gray circles denote the observations. Colored lines denote the simulations with threshold values of the D_P/D_{BC} ratio of 1.5 (blue), 1.6 (red), and 1.7 (black), where D_P and D_{BC} are the diameters of the particle and BC core, respectively. Note that ΔSO_4^{2-} amounts in both observations and model simulations are total bulk amounts including both coating materials of BC-containing and BC-free particles. (a) Comparison for BC core diameters (D_{BC}) of 100–200 nm (model) and 155–185 nm (observation). (b) Comparison for BC core diameters of 200–400 nm (model) and 210–330 nm (observation).

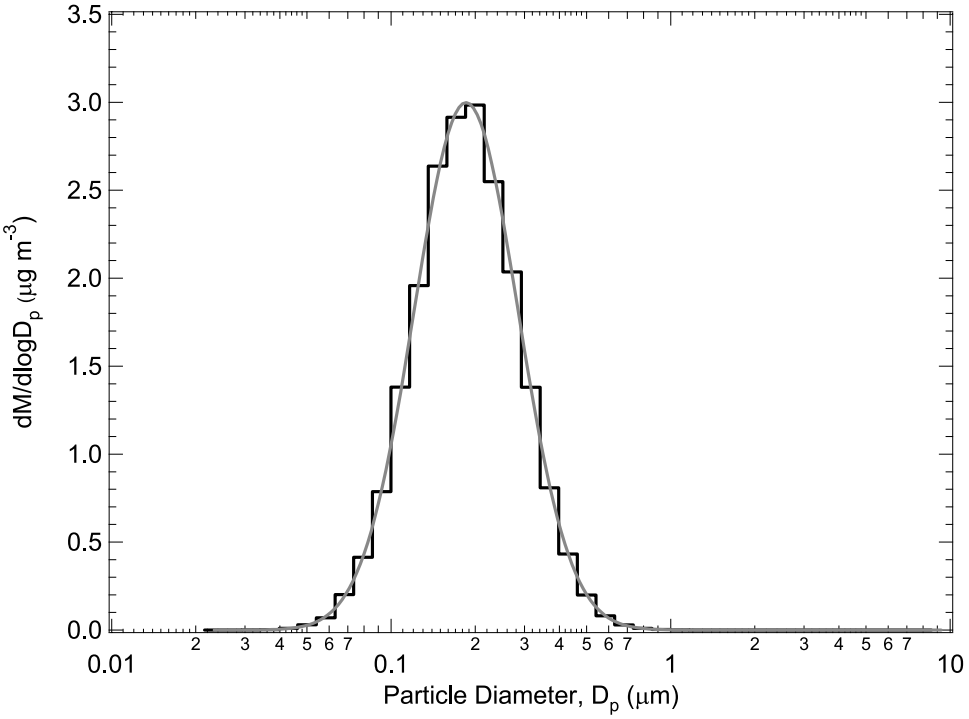

Figure 4. Mass size distribution of bare BC particles used in this study (black line). The gray line shows a lognormal function fitted to the observed size distribution in ''fresh'' air during PEACE-C flight 5.

in ''fresh'' and ''aged'' air, respectively. We note that the simulation for the first regime is necessary because the BC mixing state in ''fresh'' air cannot be uniquely constrained by observations. The SP2 instrument provides $f_{thick}(D_{BC})$ values for limited BC core diameters; however, it does not provide information on the coating thickness of individual BC-containing particles during PEACE-C. Consequently, one has to predict the BC mixing states in ''fresh'' air under the constraint of observed concentrations, by making reasonable assumptions.

4.1. Simulation Over the Source Region

[27] In this section, the simulation for the source region (i.e., the first regime) is described. The simulation started at 0600 LT, denoted as $t = t_0$ hereafter. Diurnal variation in photodissociation coefficients under clear-sky conditions was taken into account in the simulation. Atmospheric temperature and relative humidity were kept constant at 283 K and 45%, respectively, which were the observed values in ''fresh'' air. Gaseous concentrations of primary species, such as SO_2, NH_3, and nitrogen oxides (NO_x), were assumed to be constant throughout the simulation so as to minimize the day-to-day variation in diurnal variations of hydroxyl radical (OH) concentration and therefore production rates of inorganic aerosols. When the gaseous concentrations were available from observations in ''fresh'' air, they were given at $t = t_0$ in the simulation; when they were not available, typical urban air concentrations were assumed. For aerosol species at $t = t_0$, we assumed that only $(NH_4)_2SO_4$ particles existed as BC-free particles, and their concentration was chosen to be the same as that of the background aerosols (see section 3.2). They were assumed to have a lognormal distribution with a mass median diameter of 278 nm and a geometric standard deviation of 1.41, which were derived from the size distribution of BC-free particles observed in ''fresh'' air. The model simulation was performed with continuous emissions of BC and POA particles and it was truncated when the predicted bulk aerosol mass concentration of SO_4^{2-} agreed with those observed in ''fresh'' air, and this time step is expressed as $t = t_{fresh}$ hereafter.

[28] In the simulation, emissions of bare BC particles (100% BC mass fraction) were injected into the grid cells with the 90–100% BC mass fraction. These emissions took place continuously with time, and the emission rate was chosen so that the integrated BC amount added between $t = t_0$ and $t = t_{fresh}$ became equal to the BC mass concentration observed in ''fresh'' air. The size distribution of BC particles emitted was constructed by referring to that observed in ''fresh'' air (see Figure 4): a lognormal mass size distribution with a mass median diameter of 185 nm and a geometric standard deviation of 1.53. Because MADRID-BC does not include coagulation, the BC size distribution did not change throughout the simulation. Model simulations in this study were performed to predict changes in BC mixing states at urban-to-regional scales, and therefore the use of the BC core size distribution observed in ''fresh'' air is considered to be reasonable.

[29] POA particles were emitted concurrently with BC particles in the simulation. The emission rate of POA was chosen so that the emission ratio between POA and BC was equal to the observed POA/BC mass ratio in the Tokyo urban area (see Appendix A3). The POA particles were introduced as BC-free particles in the simulation, so that they were externally mixed with BC particles. The size distribution of POA particles was assumed to be the same as that of bare BC particles, although some of them were considered to be internally mixed with BC in diesel exhaust

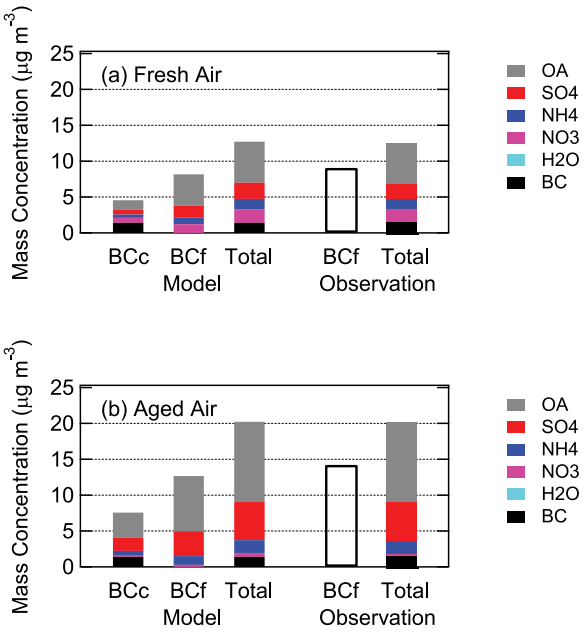

Figure 5. Model-predicted and observed bulk aerosol mass concentrations in (a) "fresh" and (b) "aged" air parcels. For model-predicted values, the concentrations of BC-containing particles (BCc) and BC-free particles (BCf) and their total values (Total) are shown separately. For observed values, the concentrations of BCf particles and the total are shown. The bulk amounts of BCf were obtained from the SP2 experiment. Total bulk aerosol amounts of individual chemical compositions (Total) were obtained from the PILS experiment. Observed values in "aged" air are the concentrations normalized to "fresh" air conditions calculated using equation (3).

[*Sakurai et al.*, 2003; *Wehner et al.*, 2004]. Results from a sensitivity simulation in which freshly emitted BC particles are partly coated with POA on emission are presented in Appendix A1.

[30] As described in section 3.2, observations suggest that SOA played an important role for BC coatings. However, we did not include condensation/evaporation of SOA in the dynamic approach in MADRID-BC because SOA was severely underestimated by model simulations, such as the CMAQ-MADRID model [e.g., *Matsui et al.*, 2009]. Therefore we used an alternative approach to treat condensation of SOA in this study. During flight 5, a linear relationship was observed between ΔWSOC/ΔBC and $\Delta SO_4^{2-}/\Delta$BC ratios (r^2 = 0.76, not shown), suggesting that SOA and SO_4^{2-} had been concurrently produced from individual precursor gases. It is therefore more or less reasonable to assume that distributions of condensed mass over different size particles were similar between SOA and SO_4^{2-}. In this study, the bulk SOA concentration in "fresh" air was estimated from the observed WSOC concentration in "fresh" air using the SOA-WSOC relationship obtained in the Tokyo urban area (see Appendix A3). The estimated SOA mass was distributed over particles so that the relative fractions of condensed SOA among particles became equal to those of SO_4^{2-} at $t = t_{fresh}$.

[31] In Figure 5a, the bulk mass concentrations of various aerosol compounds predicted at $t = t_{fresh}$ are shown with those observed in "fresh" air. The model simulations agree well with the observations because the simulations continued until the SO_4^{2-} amount agreed with observations, and various parameters were chosen so that the predicted aerosol concentrations agreed with those observed. In Figure 5a, predicted aerosol concentrations of BC-containing and BC-free particles are also shown separately, although this information was not available from the observations. It is found that model simulations reproduced well the observed total mass of BC-free particles (within a 3.0% difference), which was derived from the SP2 measurement. We note that it is essential to take into account BC-free particles for predictions of BC mixing states. Because BC-free particles serve as sites for condensation of inorganic species and SOA, they affect the coating amounts on BC particles. In fact, 66% of the total SO_4^{2-} produced owing to photochemical oxidation of SO_2 was partitioned onto the BC-free particles at $t = t_{fresh}$ in this case. This result indicates that BC-free particles in background air and those emitted as POA affect BC mixing states in the atmosphere.

[32] The predicted entire BC mixing state (BC mass distribution as a function of both BC core diameter and BC mass fraction) at $t = t_{fresh}$ is shown in Figure 6a. As shown in Figure 6a, BC-containing particles with different BC mass fractions (coating thicknesses) coexist for individual BC core diameters. Aerosols with smaller BC mass fractions (greater coating fractions) were emitted into the air (introduced into the model) near the beginning of the simulation ($t = t_0$), while those with greater BC mass fractions (smaller coating fractions) were emitted near the end of the simulation ($t = t_{fresh}$). The mass of BC particles is concentrated around 200 nm in BC core diameter, reflecting the input BC core size distribution (Figure 4). Aerosols with smaller BC core diameters grow faster, and this feature is consistent with the condensation theory described in section 2.2. As will be discussed in section 4.3, these results generally reproduced the observed $f_{thick}(D_{BC})$ values in "fresh" air well.

4.2. Simulation in the Outflow Region

[33] In this section, the simulation for the outflow region over the ocean (i.e., the second regime) is described. In order to compare the changes in BC mixing state from "fresh" to "aged" air parcels during flight 5 between simulations and observations, it is necessary to derive observed concentrations in which dilution effects are excluded, because dilution effects are not included in MADRID-BC. In this study, concentrations normalized to "fresh" air conditions, X*, are defined for various observed species X as follows:

$$X^* = \frac{\Delta X}{\Delta BC} \times \Delta BC_{fresh} + X_{background}, \qquad (3)$$

where ΔX and ΔBC are differences between observed and background concentrations of X and BC in individual air parcels, respectively, ΔBC_{fresh} is the ΔBC value in "fresh" air, and $X_{background}$ is the background concentration of X. Increases (or decreases) in X* values indicate secondary aerosol production (or loss).

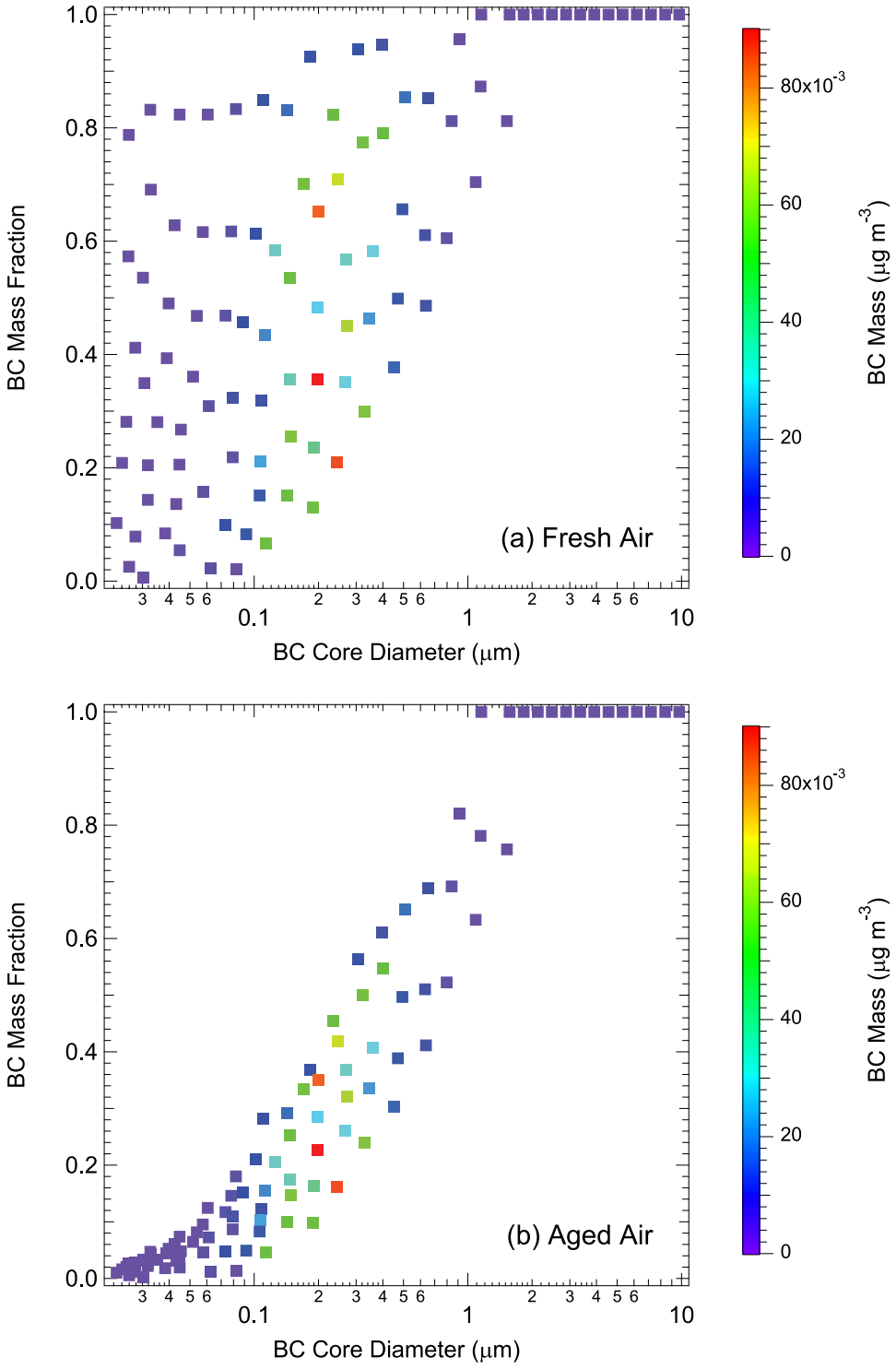

Figure 6. Predicted entire BC mixing state (BC mass distribution as a function of BC core diameter and BC mass fraction) in (a) "fresh" and (b) "aged" air parcels. The BC mass concentrations of individual grid cells are denoted by colored squares.

[34] The simulation for the outflow region over the ocean was performed using the results for "fresh" air ($t = t_{fresh}$), described in section 4.1, as an initial condition. In contrast to the simulation over the source region, emissions of BC and POA were not provided, and concentrations of gaseous species, such as SO_2, NH_3, and NO_x, changed with time as chemical reactions and condensation/evaporation proceeded. The MADRID-BC simulation started from $t = t_{fresh}$ and continued until the bulk amount of predicted SO_4^{2-} agreed with the observed SO_4^{2-}* amount defined by equation (3) in "aged" air, and this time step is denoted as $t = t_{aged}$ hereafter.

[35] As MADRID-BC does not treat the condensation/evaporation of SOA, SOA amounts were distributed over

particles in a way similar to that used for the source region simulation as follows. SOA amounts were estimated from observed WSOC concentrations using the SOA-WSOC relationship obtained in the Tokyo urban area (see Appendix A3). The estimated total SOA amounts were distributed over particles so that the relative fractions of condensed SOA among particles became equal to those of SO_4^{2-} between $t = t_{fresh}$ and $t = t_{aged}$.

[36] In Figure 5b, bulk mass concentrations of aerosol species predicted at $t = t_{aged}$ are shown with those observed in "aged" air. Note that the observed values were normalized by taking into account the dilution effect using equation (3) so that they can be directly compared with model simulations as well as the values in "fresh" air. Predicted total bulk amounts of SO_4^{2-} and OA agree with those observed because of the simulation approach used in this study. The predicted total bulk amount of NH_4^+ agrees well with observations because all of the SO_4^{2-} was neutralized by NH_4^+ in both the simulations and observations. The predicted total bulk amount of NO_3^- also agrees with observation in "aged" air. In Figure 5b, predicted aerosol concentrations of BC-containing particles and those of BC-free particles are also shown separately. The model simulations successfully reproduced the observed total amounts of BC-free particles (within a 10% difference). During transport from $t = t_{fresh}$ to $t = t_{aged}$, 58% of the condensed materials produced in the atmosphere were partitioned onto BC-free particles, indicating again the importance of the presence of BC-free particles for BC mixing states. The agreement both in the total bulk amounts and BC-free particles indicates that the amounts of inorganic and OA species in BC-containing particles were also reproduced well. Results presented in Figures 5a and 5b indicate that SO_4^{2-} and SOA were the dominant chemical composition of BC coating materials in air influenced for this particular case.

[37] The predicted entire BC mixing state at $t = t_{aged}$ is shown in Figure 6b. Compared to the entire BC mixing state at $t = t_{fresh}$ (Figure 6a), there are two distinct features. First, BC mass fractions are systematically smaller for particles with BC core diameters smaller than 1 μm at $t = t_{aged}$. Decreases in BC mass fractions are greater for smaller BC particles. For example, for particles with BC core diameters smaller than 100 nm, their BC mass fractions are smaller than 20% at $t = t_{aged}$. Second, a spread in BC mass fraction within individual BC core diameters is systematically smaller at $t = t_{aged}$. These two features result from both the condensation theory that the rate of change in a particle diameter is greater for a smaller particle and also the absence of BC emissions in the outflow region over the ocean (between $t = t_{fresh}$ and $t = t_{aged}$), in contrast to the presence of continuous bare BC emissions over the source region (between $t = t_0$ and $t = t_{fresh}$). For particles with BC core diameters greater than 2 μm, detectable change did not take place even in "aged" air.

4.3. Comparison of BC Mixing States With Observations

[38] Predicted $f_{thick}(D_{BC})$ values as a function of the $\Delta SO_4^{2-}/\Delta BC$ ratio are compared with observations for two selected BC core diameter (D_{BC}) ranges in Figures 3a and 3b. In Figures 3a and 3b, slightly wider BC core diameter ranges are adopted for the predicted values in order to minimize fluctuations in the simulations: in Figure 3a, predicted and observed values are shown for a D_{BC} of 100–200 and 155–185 nm, respectively, and in Figure 3b, predicted and observed values are shown for a D_{BC} of 200–400 and 210–330 nm, respectively. As described in section 3.1, there is uncertainty in the threshold D_P/D_{BC} ratio in discriminating thinly and thickly coated BC particles, and therefore model results are shown for three threshold D_P/D_{BC} ratios, 1.5, 1.6, and 1.7. We note that the ΔSO_4^{2-} amounts used for the horizontal axes in Figures 3a and 3b are total amounts including both BC-containing and BC-free particles.

[39] As shown in Figure 3a (D_{BC} of 155–185 nm in the observations), observed $f_{thick}(D_{BC})$ values increased with the increase in $\Delta SO_4^{2-}/\Delta BC$ ratio, and this feature was reproduced well by MADRID-BC, especially when a threshold value of D_P/D_{BC} of 1.6 was adopted. Figure 3b (D_{BC} of 210–330 nm in observation) shows that the observed increase in $f_{thick}(D_{BC})$ values was quite small, and this feature was also reproduced well by the model simulations, although the values were generally underpredicted. The smaller increase in $f_{thick}(D_{BC})$ values for larger particles can be interpreted by the condensation theory that the rate of change in BC mass fraction is smaller for larger particles, as already illustrated in Figures 6a and 6b. We note that the increase in $f_{thick}(D_{BC})$ values with the increase in the bulk $\Delta SO_4^{2-}/\Delta BC$ ratio depends not only on the entire BC mixing state (sizes and BC mass fractions of particles) but also the presence of BC-free particles, because the condensation onto BC-free particles slows the condensational growth of BC-containing particles. Therefore, the quantitative agreements between predicted and observed increases in $f_{thick}(D_{BC})$ values for the different D_{BC} ranges can be achieved only when these factors are successfully reproduced in the model simulations.

[40] The increase in $f_{thick}(D_{BC})$ values shown in Figures 3a and 3b should not be viewed as the growth of one particle. The temporal evolution of $f_{thick}(D_{BC})$ values for a given BC core diameter depends on the BC mass distribution over the entire range of BC mass fractions. This situation is more easily understood by comparing predicted BC mass distributions as a function of BC mass fraction between $t = t_{fresh}$ and $t = t_{aged}$. The comparisons are shown for BC core diameters of 100–200 (Figure 7a) and 200–400 nm in Figure 7b. The BC mass distributions shown in Figures 7a and 7b were extracted from those shown in Figures 6a and 6b. As shown in Figure 7a (D_{BC} of 100–200 nm), the distribution of BC mass at $t = t_{fresh}$ is more or less uniform over the entire range of BC mass fractions, while at $t = t_{aged}$, all the BC-containing particles have BC mass fractions smaller than 0.4. When a threshold D_P/D_{BC} ratio of 1.6 is adopted, which is equivalent to a BC mass fraction of 0.25 (dashed line in Figure 7a), the numerator of the $f_{thick}(D_{BC})$ value (see equation (2)) corresponds to the sum of the BC mass for particles with BC mass fractions smaller than 0.25 (e.g., left-hand side of the dashed line in Figure 7a). On the other hand, the denominator of the $f_{thick}(D_{BC})$ value corresponds to the total BC mass integrated over all BC mass fractions for particles having a given BC core diameter. As the condensation process proceeds, particles with BC mass fractions greater than 0.25 (e.g.,

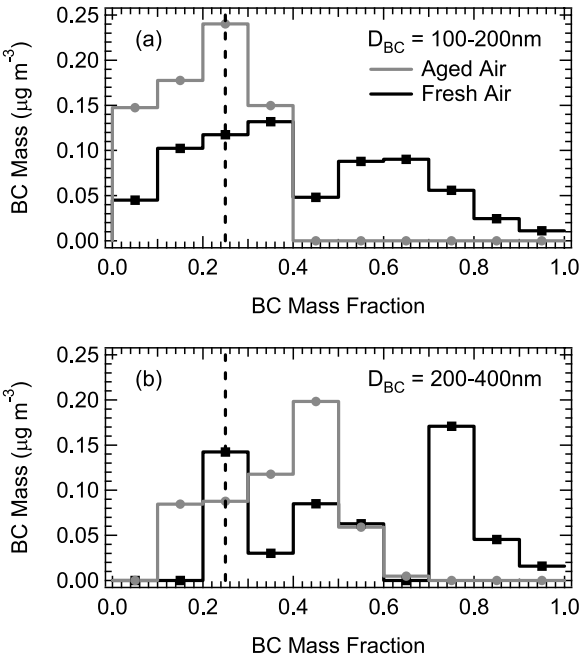

Figure 7. Predicted BC mass distributions as a function of BC mass fraction for (a) BC core diameters of 100–200 nm and (b) those of 200–400 nm. Black and gray lines denote distributions in "fresh" and "aged" air, respectively. Vertical dashed lines denote the threshold value of D_P/D_{BC} of 1.6, where D_P and D_{BC} are the diameters of the particle and the BC core, respectively.

right-hand side of the dashed line in Figure 7a) move to the left-hand side. This transition corresponds to the increase in the $f_{thick}(D_{BC})$ values shown in Figure 3a, from 0.25 at $t = t_{fresh}$ t_{fresh} to 0.66 at $t = t_{aged}$. The relatively uniform BC mass distribution with respect to the BC mass fraction at $t = t_{fresh}$ shown in Figure 7a leads to a steady increase in the $f_{thick}(D_{BC})$ value with the increase in $\Delta SO_4^{2-}/\Delta BC$ ratio, as shown in Figure 3a. Similarly, the slow movement of the BC mass distribution found for BC core diameters of 200–400 nm between $t = t_{fresh}$ and $t = t_{aged}$ (Figure 7b) corresponds to the small increase in the $f_{thick}(D_{BC})$ values shown in Figure 3b. Consequently, the agreement in $f_{thick}(D_{BC})$ values between model simulations and observations suggests the validity of the model simulations for BC mass distributions over the entire range of BC mass fractions for the given BC core ranges. Although the predicted entire BC mixing state cannot be validated directly owing to the limits of the information available from the observations, the agreement in the time evolution of the $f_{thick}(D_{BC})$ values provides some basis for validation of the BC mixing states predicted by MADRID-BC. The results presented above indicate that the evolution of BC mixing states can be interpreted at least by the condensational growth process for this particular case, although contributions of coagulation may also be important under certain circumstances. The contribution of coagulation cannot be quantified in this study because the coagulation process is not included in MADRID-BC. Instead, a simple evaluation of its effect was made for our particular case and is presented in Appendix A2.

4.4. Average Growth Ratio of BC-Containing Particles

[41] To examine aerosol mass distribution as a function of BC core diameter, the sum of the predicted aerosol mass for particles within selected BC core diameter ranges are shown for both "fresh" ($t = t_{fresh}$) and "aged" air parcels ($t = t_{aged}$) in Figure 8a. Although particles with different coating amounts (BC mass fractions) coexist in individual BC core diameter ranges, the total amounts integrated over particles within the individual BC core ranges are shown in Figure 8a. The mass distribution of BC cores itself is also shown for comparison (dashed line). In order to minimize fluctuations, the values are shown for six BC core diameter ranges, although 40 particle size sections were employed in this study (section 2.1). As shown in Figure 8a, the maximum coating amount (i.e., difference between the mass of the particle and that of the BC core) is found in the BC core diameter range of 0.1–0.2 μm, where the maximum BC mass is found (dashed line in Figure 8a). This is because the surface area of BC particles is the maximum in this BC core range.

[42] To characterize the growth ratio of BC-containing particles, the average growth ratio of particle diameters

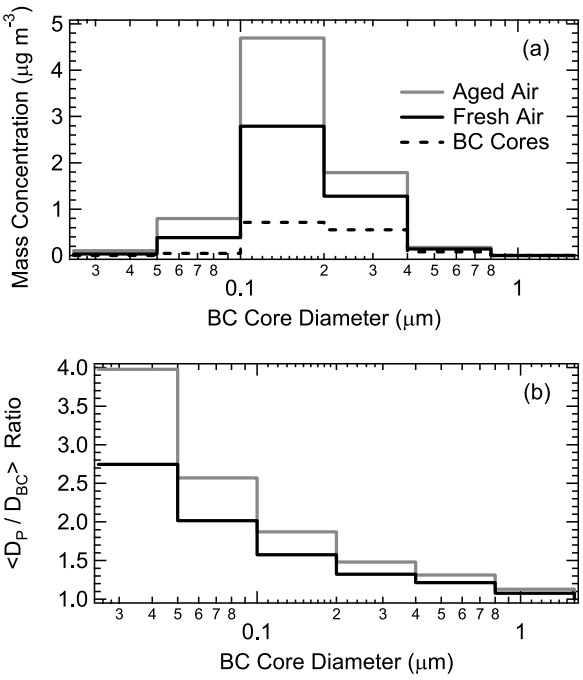

Figure 8. (a) Predicted aerosol mass distribution of BC-containing particles as a function of BC core diameter. The sum of aerosol mass for particles within the selected BC core diameter ranges is shown. (b) Distribution of the average growth ratio of particle diameter $\langle D_P/D_{BC}\rangle$, defined by equation (4), as a function of BC core diameter. Black and gray solid lines denote values for "fresh" and "aged" air, respectively. Dashed lines in Figure 8a denote the mass distribution of BC cores within the selected BC core diameter ranges.

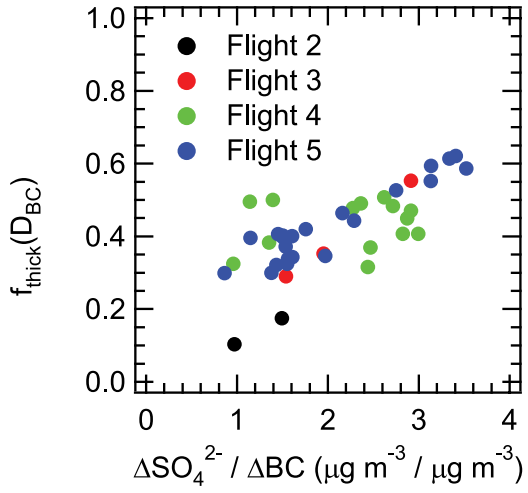

Figure 9. Mass fraction of thickly coated BC particles, $f_{thick}(D_{BC})$, defined by equation (2), as a function of the bulk $\Delta SO_4^{2-}/\Delta BC$ ratio in air parcels observed during the entire PEACE-C period. The $f_{thick}(D_{BC})$ values are shown for a BC core diameter (D_{BC}) of 175–185 nm. Only air parcels that had likely been influenced by Japanese emission sources (on the basis of the back trajectories and the criterion of $\Delta BC > 0.1$ μg m^{-3}), had likely not been influenced by wet processes (air with a value of $\Delta BC/\Delta CO$ of 0.005–0.015 μg m^{-3} ppbv^{-1} and a relative humidity of smaller than 80%), and were sampled at altitudes below 2 km over the ocean are shown. All data obtained during flight 1 were excluded because of these selection criteria. Note that the bulk ΔSO_4^{2-} amounts include both coating materials of BC-containing and BC-free particles.

$\langle D_P/D_{BC}\rangle$ was calculated for the individual BC core diameter ranges as follows:

$$\left\langle \frac{D_P}{D_{BC}} \right\rangle = \left(\frac{\sum V_P}{\sum V_{BC}} \right)^{\frac{1}{3}}, \tag{4}$$

where V_P and V_{BC} are the volumes of a BC-containing particle and BC core, respectively, and the sum is calculated within the individual BC core size ranges. The average growth ratios at $t = t_{fresh}$ and $t = t_{aged}$ are shown for selected BC core diameter ranges in Figure 8b. As clearly shown in Figure 8b, the average growth ratios are greater for particles with smaller BC core diameters, and these features were already described using Figures 6a and 6b. For example, a maximum of the $\langle D_P/D_{BC}\rangle$ ratio of 4.0 is found for BC core ranges of 0.025–0.05 μm at $t = t_{aged}$. The $\langle D_P/D_{BC}\rangle$ ratio of particles with a BC core range of 0.1–0.2 μm, where the maximum values of both BC mass and its coatings are found, increased from 1.6 at $t = t_{fresh}$ to 1.9 at $t = t_{aged}$ during transport. The contrast in BC core size dependence shown in Figures 8a and 8b indicates that although the growth ratio of a single particle is greater for smaller particles, the size distribution of bare BC particles controls the distribution of coating amounts over BC particles, suggesting the importance of BC size distribution on BC mixing state.

4.5. BC Aging Observed in Other Outflows

[43] The model simulations described in previous sections were performed so that their results could be compared with particular observations (flight 5) conducted during the PEACE-C aircraft measurements. Simulations for the two regimes were performed in this study, namely the source region regime (coating process concurrent with continuous BC and POA emissions) and the outflow region regime (coating process without the emissions). The simulations for these two regimes are considered to be representative of the general situation of BC aging processes in air transported from anthropogenic sources, although the assumptions made for these two regimes are rather simple. In this section, the generality of the simulations performed for flight 5 is discussed.

[44] In Figure 9, observed mass fractions of thickly coated BC particles, $f_{thick}(D_{BC})$, are shown as a function of the $\Delta SO_4^{2-}/\Delta BC$ ratio using all data obtained in the PBL over the ocean during the PEACE-C aircraft measurements (flights 2 to 5). In Figure 9, we selected only air parcels that had likely been influenced by Japanese emission sources (on the basis of back trajectories) and had likely not been influenced by wet processes during transport (with a value of $\Delta BC/\Delta CO$ of 0.005–0.015 μg m^{-3} ppbv^{-1} and a relative humidity lower than 80%). In general, a similar tendency between $f_{thick}(D_{BC})$ values and $\Delta SO_4^{2-}/\Delta BC$ ratios is found among data obtained from these four flights. This result suggests that air parcels transported from anthropogenic sources in Japan to the ocean generally undergo a similar evolution of BC mixing states when air parcels are not influenced by wet processes. Because the $f_{thick}(D_{BC})$ values as a function of the $\Delta SO_4^{2-}/\Delta BC$ ratio are reproduced well by MADRID-BC for flight 5 (e.g., Figure 3a), the results obtained by the model simulations for flight 5 also agree with the other observations conducted around Japan. Consequently, the BC mixing states obtained by the simulations for flight 5 are considered to have features typical of air influenced by anthropogenic sources in Japan during the PEACE-C period.

[45] Note that even when the $\Delta SO_4^{2-}/\Delta BC$ ratio is the same in different air parcels, the BC mixing states can be different, depending on various factors, such as the BC core size distribution, initial BC mixing state in the emissions, the presence of BC-free particles, the relative contributions of coating amounts between the source region and outflow region, relationships of the production of sulfate and other aerosol compounds (e.g., OA), coagulation processes, wet removal processes, and the aqueous-phase production of sulfate. The similarities in the BC mixing states shown in Figure 9 suggest that these factors and conditions are generally similar for air parcels influenced by sources over Japan in our particular cases. Although the number of cases shown in Figure 9 is limited, the results presented in this study suggest that the $\Delta SO_4^{2-}/\Delta BC$ ratio can be a useful parameter to estimate BC mixing states in outflow from anthropogenic sources.

5. Summary and Conclusions

[46] In this study, a new box model, MADRID-BC, was developed to accurately simulate the time evolution of the entire BC mixing state, namely the size distribution of BC cores and mass concentrations of their coating material, resulting from condensation/evaporation processes. In this model, a 2-D aerosol representation in which aerosol mass

and number are given for individual particle diameters and BC mass fractions is incorporated into the MADRID aerosol module, following the method of *Jacobson* [2001]. In addition to BC-containing particles, BC-free particles are treated separately in this model. An accurate mass transfer algorithm was also implemented into the model to partition condensable compounds between coexisting BC-containing and BC-free particles with different particle diameters.

[47] To validate the MADRID-BC box model, the model was applied to flight 5 of the PEACE-C aircraft measurements conducted around Japan in March 2004. During flight 5, the Lagrangian time evolution of the mass fraction of thickly coated BC particles, $f_{thick}(D_{BC})$, defined by equation (2), was observed using an SP2 instrument in air parcels on a timescale of 2 (''fresh'' air) to 13 (''aged'' air) hours during horizontal transport from the Nagoya urban area within the PBL over the ocean [*Moteki et al.*, 2007]. In order to reproduce the observed time evolution of the $f_{thick}(D_{BC})$ values from ''fresh'' to ''aged'' air parcels, simulations for two consecutive regimes were performed using MADRID-BC. The simulation in the first regime was for the source region, where continuous emissions of BC and POA particles and a concurrent coating process took place. The simulation in the second regime, which follows the first regime simulation, was for the outflow region over the ocean, where the coating process without the emissions took place. These simulations were performed using observed bulk amounts of aerosols and gaseous concentrations as constraints so that the predicted bulk $\Delta SO_4^{2-}/\Delta BC$ ratio became equal to that observed in ''fresh'' ($t = t_{fresh}$) and ''aged'' air ($t = t_{aged}$), respectively.

[48] MADRID-BC reproduced well the observed increase in $f_{thick}(D_{BC})$ values with the increase in the $\Delta SO_4^{2-}/\Delta BC$ ratios in air transported over the ocean (between $t = t_{fresh}$ and $t = t_{aged}$) for the observed BC core diameter ranges. The agreement in $f_{thick}(D_{BC})$ values between model simulations and observations suggests the validity of the model simulations for BC mass distributions over the entire BC mass fraction range, although this evaluation is conducted with particular observations, and more comprehensive comparisons are needed. The validity found in this study suggests that general features of the evolution of BC mixing states can be interpreted at least by the condensational growth process in this particular case, although the contribution of coagulation was not quantified in this study. The model simulations also show that the observed BC evolution can be reproduced only when SOA is taken into account as coating materials, indicating their importance for the BC mixing state. In our simulations, 58% of the total condensed amount produced between $t = t_{fresh}$ and $t = t_{aged}$ was partitioned onto BC-free particles, indicating that the presence of BC-free particles significantly slowed down the condensational growth of BC-containing particles.

[49] We examined the changes in the coating thickness of BC-containing particles in air parcels from ''fresh'' to ''aged'' air conditions predicted by MADRID-BC in order to obtain insights into the entire BC mixing state. At $t = t_{fresh}$, BC-containing particles having various coating thicknesses coexisted for individual BC core diameters, which were smaller than 1 μm. On the other hand, at $t = t_{aged}$, the spread in the coating thickness of the BC-containing particles within individual BC core diameters was systematically smaller. The average growth ratio of particle diameter $\langle D_P/D_{BC} \rangle$, defined by equation (4), increased from 1.6 at $t = t_{fresh}$ to 1.9 at $t = t_{aged}$ for particles with BC core diameters of 100–200 nm, where both the maximum mass of BC and its coating materials were found. Although the growth ratio was found to be greater for smaller BC particles, the size distribution of bare BC particles controlled the distribution of coating amounts over BC particles.

[50] The BC mixing states obtained by the MADRID-BC simulations for flight 5 are considered to represent typical air influenced by anthropogenic sources in Japan during the PEACE-C period. This is because the predicted relationship between $f_{thick}(D_{BC})$ values and the bulk $\Delta SO_4^{2-}/\Delta BC$ ratios agreed well with that observed in air parcels within the PBL over the ocean during all the flights in PEACE-C when the air parcels had likely been influenced by Japanese emission sources and had likely not experienced wet processes.

[51] This study examines the temporal evolution of the entire BC mixing state in outflow from Japanese anthropogenic sources using MADRID-BC. This information is necessary and sufficient to calculate accurately aerosol optical properties and CCN activities and contributes to improving the estimation of the effects of BC on climate. The influences of BC mixing states on aerosol optical properties and CCN activities are further explored in a companion paper (Oshima et al., submitted manuscript, 2008). These modeling studies of BC using a BC-mixing-state-resolved model are particularly important for the Asian region, which includes large BC emission sources.

Appendix A

A1. A Sensitivity Simulation With Freshly Emitted BC Particles Having Organic Coatings

[52] In this study, BC particles emitted into the atmosphere are assumed to be bare (100% BC mass fraction) as described in section 4.1 (referred to as ''base case'' simulations, hereafter). To address uncertainties associated with the mixing states of freshly emitted BC particles, a sensitivity simulation was performed.

[53] In general, particles from diesel exhaust contain both BC and OM, and some BC particles may be internally mixed with OM. A recent study made by *Wehner et al.* [2004] showed that there were two types of BC-containing particles from vehicular traffic emissions in Germany, namely less-coated BC particles (i.e., the thickness of the volatile layer (organics) is less than 10% of the particle radius) and more-coated BC particles (i.e., the thickness is greater than 10% of the particle radius). They showed that about 90% and 10% of BC volume of total BC-containing particles were in the form of less-coated and more-coated BC particles, respectively. OM emitted together with BC is considered to partly exist as externally mixed particles.

[54] In the sensitivity simulation, we assumed that 90% and 10% of BC mass was included in particles with BC mass fractions greater and smaller than 75% (which is equivalent to a D_P/D_{BC} ratio of 1.1), respectively, upon emission, based on the results of *Wehner et al.* [2004]. Because initial distributions of the coating thickness of BC-containing particles are not available from the measure-

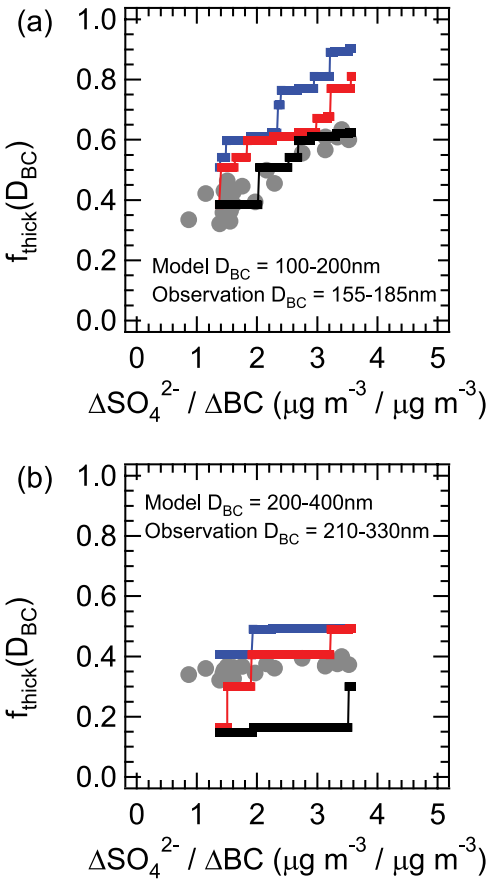

Figure A1. Same as Figure 3 but for a sensitivity simulation in which freshly emitted BC particles are assumed to be partly coated with organics. See the text for details.

ments, we made the following assumptions. We assumed a uniform distribution of BC particles over BC mass fractions for each of two BC mass fraction ranges, namely, 75–100% and 0–75%, and these BC particles were assumed to be coated with POA. From this assumption, the amounts of POA internally mixed with BC were derived. Because the BC-to-total POA mass ratio was fixed in this study (Appendix A3), the rest of POA was assumed to be in the form of externally mixed BC-free particles in the simulation. As a consequence, the amount of POA in BC-free particles became smaller by 29% as compared with that for the "base case" simulations. Other than the assumptions of the mixing state of freshly emitted BC and POA, the sensitivity simulation used the same input and calculation procedures as those used for the "base case" simulations.

[55] Predicted $f_{thick}(D_{BC})$ values, defined by equation (2), as a function of the bulk $\Delta SO_4^{2-}/\Delta BC$ ratio are compared with observations for two selected BC core diameter ranges in Figures A1a (D_{BC} of 100–200 nm) and A1b (D_{BC} of 200–400 nm). Compared with "base case" simulations (i.e., Figures 3a and 3b), predicted $f_{thick}(D_{BC})$ values are systematically greater because greater amounts of coating materials condensed on BC-containing particles. However, as shown in Figure A1a (D_{BC} of 100–200 nm), the observed increase in $f_{thick}(D_{BC})$ values with the increase in $\Delta SO_4^{2-}/\Delta BC$ ratio is reproduced well, when a threshold value of D_P/D_{BC} of 1.7 is adopted. For D_{BC} of 200–400 nm (Figure A1b), the observed small increase in $f_{thick}(D_{BC})$ values was also more or less reproduced by the sensitivity simulation. The average growth ratios of particle diameters $\langle D_P/D_{BC}\rangle$, defined by equation (4), were greater by about 10% than those of "base case" simulations (Figure 8b) for particles with both size ranges.

[56] Although the growth ratios and hence the coating thicknesses of individual BC-containing particles are not significantly different from those of the "base case" simulations for this particular case, more laboratory and/or observational studies on the mixing states of freshly emitted BC particles are needed in order to reduce uncertainties in the BC mixing state in the atmosphere.

A2. Possible Contributions of Coagulation

[57] Possible contributions of coagulation to the BC mixing state in air sampled during flight 5 are examined in this appendix. In "fresh" air, the median diameter of the number size distributions of both bare BC particles and BC-free particles is approximately 100 nm. The number concentration of BC-free particles in "fresh" air is 4400 cm^{-3}, which is about a factor of 10 greater than that of BC particles. The Fuchs form of the Brownian self-coagulation coefficient for monodisperse particles with a diameter of 100 nm is 1.5×10^{-9} cm^3 s^{-1} [*Seinfeld and Pandis*, 2006]. Assuming that both BC and BC-free particles have monodisperse size distributions with a diameter of 100 nm, the timescale for individual BC particles to collide with another (BC or BC-free) particle is estimated to be 42 h. When dilution of air during transport is taken into account, this timescale becomes even longer. Considering a transport time of air between "fresh" and "aged" air parcels of approximately a half day, estimated from the trajectory calculations (section 3.2), the effect of coagulation on BC mixing state is considered to be small.

A3. Estimation of POA and SOA Amounts

[58] In this study, POA and SOA mass concentrations were estimated using observed BC and WSOC concentrations, respectively. *Miyazaki et al.* [2006] showed that the diurnally averaged water-insoluble organic carbon-to-BC ratios (WIOC/BC) were nearly constant (1.1 ± 0.1 μgC/μgC) in the Tokyo urban area throughout the year. Using this ratio, WIOC concentrations in individual air parcels were estimated from observed BC concentrations. On the other hand, *Kondo et al.* [2007] reported observed values of both HOA/WIOC and OOA/WSOC ratios in the Tokyo urban area in summer and winter, where HOA and OOA denotes hydrocarbon-like organic aerosol and oxygenated organic aerosol, respectively. Because the PEACE-C mission was conducted in spring (late March), ratios in summer and winter were averaged so that a HOA/WIOC value of 1.2 μg/μgC and a OOA/WSOC value of 3.2 μg/μgC were obtained. Using these relationships, the HOA and OOA concentrations were calculated from observed BC and WSOC concentrations, respectively. *Kondo et al.* [2007] also reported that the HOA and OOA concentrations observed in the Tokyo urban area generally agreed with those of POA and SOA, respectively. Therefore, in this

study, estimated HOA and OOA concentrations were used as POA and SOA concentrations, respectively.

A4. Uniformity in Air Parcels Sampled During Flight 5

[59] In this study, air parcels sampled in the PBL over the ocean during flight 5 were utilized to study the Lagrangian time evolution of BC mixing states. This approach is valid only when all air parcels were affected by similar types of emission sources and underwent similar physical and chemical processes. This point is examined in this appendix.

[60] We examined $\Delta CO/\Delta BC$ ratios where ΔCO and ΔBC are the differences between observed and background concentrations of CO and BC, respectively. Background concentrations of CO and BC were chosen to be 150 and 0 ppbv, respectively, which were the minimum values observed during flight 5. During flight 5, changes in the $\Delta CO/\Delta BC$ ratios were found to be small for most air parcels (77.8 ± 10 ppbv μg^{-1} m^3 for $\Delta BC > 0.1$ μg m^{-3}). The similarity of the $\Delta CO/\Delta BC$ ratios is consistent with the trajectory analyses described in section 3.2, showing that these air parcels were influenced by the same types of emission sources over the Nagoya urban area. The present results further suggest that wet removal, which would reduce only BC concentrations, did not take place during flight 5. Consequently, it is suggested that the changes in BC concentrations observed during flight 5 were primarily due to dilution with background air, which also reduced CO concentrations, resulting in constant $\Delta CO/\Delta BC$ ratios.

[61] A similar examination was performed for the $\Delta SO_x/\Delta BC$ ratios. Background concentrations of SO_2 and SO_4^{2-} were chosen to be 0 and 0.1 ppbv, respectively, which were the minimum values observed during flight 5. The changes in the $\Delta SO_x/\Delta BC$ ratios were found to be small for most air parcels (1.53 ± 0.40 ppbv μg^{-1} m^3 for $\Delta BC > 0.1$ μg m^{-3}). This is again consistent with the similarity in the emission sources and the absence of wet removal.

[62] **Acknowledgments.** We are indebted to all of the PEACE-C participants for their cooperation and support. Special thanks are owed to the flight and ground crews of the DAS GII aircraft for helping make this effort into a success. We express our appreciation to Y. Komazaki for his help with the PEACE-C aircraft measurements and providing the BC data measured by HI-PSAP. We thank S. Hatakeyama for providing the SO_2 data. This study was supported by the Ministry of Education, Culture, Sports, Science, and Technology (MEXT) and the global environment research fund of the Japanese Ministry of the Environment (B-083). The EORC of JAXA supported the PEACE campaigns. This study was conducted as a part of the Mega-Cities: Asia Task under the framework of the International Global Atmospheric Chemistry (IGAC) project. The trajectory calculation program used in this paper was developed by Y. Tomikawa of the National Institute of Polar Research and K. Sato of the University of Tokyo, Japan. N. Oshima was supported by Research Fellowships of the Japan Society for the Promotion of Science (JSPS) for Young Scientists. Y.Z. at North Carolina State University was supported by the United State National Science Foundation Career Award Atm-0348819.

References

Ackerman, A. S., O. B. Toon, D. E. Stevens, A. J. Heymsfield, V. Ramanathan, and E. J. Welton (2000), Reduction of tropical cloud cover by soot, *Science*, *288*, 1042–1047, doi:10.1126/science.288.5468.1042.

Baumgardner, D., G. Kok, and G. Raga (2004), Warming of the Arctic lower stratosphere by light absorbing particles, *Geophys. Res. Lett.*, *31*, L06117, doi:10.1029/2003GL018883.

Bey, I., D. J. Jacob, J. A. Logan, and R. M. Yantosca (2001), Asian chemical outflow to the Pacific in spring: Origins, pathways, and budgets, *J. Geophys. Res.*, *106*, 23,097–23,113, doi:10.1029/2001JD000806.

Bhattacharjee, P. S., A. K. Prasad, M. Kafatos, and R. P. Singh (2007), Influence of a dust storm on carbon monoxide and water vapor over the Indo-Gangetic Plains, *J. Geophys. Res.*, *112*, D18203, doi:10.1029/2007JD008469.

Bohren, C. F., and D. R. Huffman (1983), *Absorption and Scattering of Light by Small Particles*, John Wiley, Hoboken, N. J.

Bond, T. C., D. G. Streets, K. F. Yarber, S. M. Nelson, J.-H. Woo, and Z. Klimont (2004), A technology-based global inventory of black and organic carbon emissions from combustion, *J. Geophys. Res.*, *109*, D14203, doi:10.1029/2003JD003697.

Bond, T. C., G. Habib, and R. W. Bergstrom (2006), Limitations in the enhancement of visible light absorption due to mixing state, *J. Geophys. Res.*, *111*, D20211, doi:10.1029/2006JD007315.

Byun, D. W., and J. K. S. Ching (1999), Science algorithms of the EPA Models-3 Community Multiscale Air Quality (CMAQ) modeling system, *EPA/600/R-99/030*, Off. of Res. and Dev., U.S. Environ. Prot. Agency, Washington, D. C.

Clarke, A. D., et al. (2004), Size distributions and mixtures of dust and black carbon aerosol in Asian outflow: Physiochemistry and optical properties, *J. Geophys. Res.*, *109*, D15S09, doi:10.1029/2003JD004378.

Croft, B., U. Lohmann, and K. von Salzen (2005), Black carbon aging in the Canadian Centre for Climate modelling and analysis atmospheric general circulation model, *Atmos. Chem. Phys.*, *5*, 131–1949.

Fast, J. D., W. I. Gustafson Jr., R. C. Easter, R. A. Zaveri, J. C. Barnard, E. G. Chapman, G. A. Grell, and S. E. Peckham (2006), Evolution of ozone, particulates, and aerosol direct radiative forcing in the vicinity of Houston using a fully coupled meteorology-chemistry-aerosol model, *J. Geophys. Res.*, *111*, D21305, doi:10.1029/2005JD006721.

Gao, R. S., et al. (2007), A novel method for estimating light-scattering properties of soot aerosols using a modified single-particle soot photometer, *Aerosol Sci. Technol.*, *41*, 125–135, doi:10.1080/02786820601118398.

Gery, M. W., G. Z. Whitten, J. P. Killus, and M. C. Dodge (1989), A photochemical kinetics mechanism for urban and regional scale computer modeling, *J. Geophys. Res.*, *94*, 12,925–12,956, doi:10.1029/JD094iD10p12925.

Grell, G. A., J. Dudhia, and D. R. Stauffer (1995), A description of the fifth-generation Penn State/NCAR mesoscale model (MM5), *NCAR/TN-398+STR*, 122 pp., Natl. Cent. for Atmos. Res., Boulder, Colo.

Hansen, J., M. Sato, and R. Reudy (1997), Radiative forcing and climate response, *J. Geophys. Res.*, *102*, 6831–6864, doi:10.1029/96JD03436.

Intergovernmental Panel on Climate Change (2007), *Climate Change 2007–The Physical Science Basis Working Group I Contribution to the Fourth Assessment Report of the IPCC Corporate Author Intergovernmental Panel on Climate Change*, Cambridge Univ. Press, Cambridge, U. K.

Jacob, D. (2000), Heterogeneous chemistry and tropospheric ozone, *Atmos. Environ.*, *34*, 2131–2159, doi:10.1016/S1352-2310(99)00462-8.

Jacobson, M. Z. (1997), Development and application of a new air pollution modeling system, part II, Aerosol module structure and design, *Atmos. Environ.*, *31*, 131–144, doi:10.1016/1352-2310(96)00202-6.

Jacobson, M. Z. (1999), *Fundamentals of Atmospheric Modeling*, Cambridge Univ. Press, New York.

Jacobson, M. Z. (2000), A physically based treatment of elemental carbon optics: Implication for global direct forcing of aerosols, *Geophys. Res. Lett.*, *27*(2), 217–220, doi:10.1029/1999GL010968.

Jacobson, M. Z. (2001), Strong radiative heating due to the mixing state of black carbon in atmospheric aerosols, *Nature*, *409*, 695–697, doi:10.1038/35055518.

Jacobson, M. Z. (2002a), Control of fossil-fuel particulate black carbon and organic matter, possibly the most effective method of slowing global warming, *J. Geophys. Res.*, *107*(D19), 4410, doi:10.1029/2001JD001376.

Jacobson, M. Z. (2002b), Analysis of aerosol interactions with numerical techniques for solving coagulation, nucleation, condensation, dissolution, and reversible chemistry among multiple size distributions, *J. Geophys. Res.*, *107*(D19), 4366, doi:10.1029/2001JD002044.

Koike, M., et al. (2003), Export of anthropogenic reactive nitrogen and sulfur compounds from the east Asia region in spring, *J. Geophys. Res.*, *108*(D20), 8789, doi:10.1029/2002JD003284.

Kondo, Y., et al. (2006), Temporal variations of elemental carbon in Tokyo, *J. Geophys. Res.*, *111*, D12205, doi:10.1029/2005JD006257.

Kondo, Y., Y. Miyazaki, N. Takegawa, T. Miyakawa, R. J. Weber, J. L. Jimenez, Q. Zhang, and D. R. Worsnop (2007), Oxygenated and water-soluble organic aerosols in Tokyo, *J. Geophys. Res.*, *112*, D01203, doi:10.1029/2006JD007056.

Koren, I., Y. J. Kaufman, L. A. Remer, and J. V. Martins (2004), Measurement of the effect of Amazon smoke on inhibition of cloud formation, *Science*, *303*, 1342–1345, doi:10.1126/science.1089424.

Liu, H., D. J. Jacob, I. Bey, R. M. Yantosca, B. N. Duncan, and G. W. Sachse (2003), Transport pathways for Asian combustion outflow over

the Pacific: Interannual and seasonal variations, *J. Geophys. Res.*, *108*(D20), 8786, doi:10.1029/2002JD003102.
Matsui, H., M. Koike, N. Takegawa, Y. Kondo, R. J. Griffin, Y. Miyazaki, Y. Yokouchi, and T. Ohara (2009), Secondary organic aerosol formation in urban air: Temporal variations and possible contributions from unidentified hydrocarbons, *J. Geophys. Res.*, *114*, D04201, doi:10.1029/2008JD010164.
Meng, Z., D. Dabdub, and J. H. Seinfeld (1998), Size-resolved and chemically resolved model of atmospheric aerosol dynamics, *J. Geophys. Res.*, *103*, 3419–3435, doi:10.1029/97JD02796.
Menon, S., J. Hansen, L. Nazarenkk, and Y. Lup (2002), Climate effects of black carbon aerosols in China and India, *Science*, *297*, 2250–2253, doi:10.1126/science.1075159.
Miyazaki, Y., et al. (2003), Synoptic-scale transport of reactive nitrogen over the western Pacific in spring, *J. Geophys. Res.*, *108*(D20), 8788, doi:10.1029/2002JD003248.
Miyazaki, Y., Y. Kondo, N. Takegawa, Y. Komazaki, K. Kawamura, M. Mochida, K. Okuzawa, and R. J. Weber (2006), Time-resolved measurements of water-soluble organic carbon in Tokyo, *J. Geophys. Res.*, *111*, D23206, doi:10.1029/2006JD007125.
Moteki, N., and Y. Kondo (2007), Effects of mixing state on black carbon measurement by laser-induced incandescence, *Aerosol Sci. Technol.*, *41*, 398–417, doi:10.1080/02786820701199728.
Moteki, N., Y. Kondo, Y. Miyazaki, N. Takegawa, Y. Komazaki, G. Kurata, T. Shirai, D. R. Blake, T. Miyakawa, and M. Koike (2007), Evolution of mixing state of black carbon particles: Aircraft measurements over the western Pacific in March 2004, *Geophys. Res. Lett.*, *34*, L11803, doi:10.1029/2006GL028943.
Nenes, A., S. N. Pandis, and C. Pilinis (1998), ISORROPIA: A new thermodynamic equilibrium model for multiphase multicomponent inorganic aerosols, *Aquat. Geochem.*, *4*, 123–152, doi:10.1023/A:1009604003981.
Nenes, A., C. Pilinis, and S. N. Pandis (1999), Continued development and testing of a new thermodynamic aerosol module for urban and regional air quality models, *Atmos. Environ.*, *33*, 1553–1560, doi:10.1016/S1352-2310(98)00352-5.
Oshima, N., et al. (2004), Asian chemical outflow to the Pacific in late spring observed during the PEACE-B aircraft mission, *J. Geophys. Res.*, *109*, D23S05, doi:10.1029/2004JD004976.
Park, K., et al. (2004), Measurement of inherent material density of nanoparticle agglomerates, *J. Nanopart. Res.*, *6*, 267–272, doi:10.1023/B:NANO.0000034657.71309.e6.
Park, R. J., et al. (2005), Export efficiency of black carbon aerosol in continental outflow: Global implications, *J. Geophys. Res.*, *110*, D11205, doi:10.1029/2004JD005432.
Prasad, A. K., and R. P. Singh (2007), Changes in aerosol parameters during major dust storm events (2001–2005) over the Indo-Gangetic basin using AERONET and MODIS data, *J. Geophys. Res.*, *112*, D09208, doi:10.1029/2006JD007778.
Prasad, A. K., R. P. Singh, and M. Kafatos (2006), Influence of coal based thermal power plants on aerosol optical properties in the Indo-Gangetic basin, *Geophys. Res. Lett.*, *33*, L05805, doi:10.1029/2005GL023801.
Ramanathan, V., P. J. Crutzen, J. T. Kiehl, and D. Rosenfeld (2001a), Aerosols, climate, and the hydrological cycle, *Science*, *294*, 2119–2124, doi:10.1126/science.1064034.
Ramanathan, V., et al. (2001b), Indian Ocean Experiment: An integrated analysis of the climate forcing and effects of the great Indo-Asian haze, *J. Geophys. Res.*, *106*, 28,371–28,398, doi:10.1029/2001JD900133.
Riemer, N., H. Vogel, B. Vogel, and F. Fiedler (2003), Modeling aerosols on the mesoscale-γ: Treatment of soot aerosol and its radiative effects, *J. Geophys. Res.*, *108*(D19), 4601, doi:10.1029/2003JD003448.
Riemer, N., H. Vogel, and B. Vogel (2004), Soot aging time scales in polluted regions during day and night, *Atmos. Chem. Phys.*, *4*, 1885–1893.
Sakurai, H., K. Park, P. H. McMurry, D. D. Zarling, D. B. Kittelson, and P. J. Ziemann (2003), Size-dependent mixing characteristics of volatile and nonvolatile components in diesel exhaust aerosols, *Environ. Sci. Technol.*, *37*, 5487–5495, doi:10.1021/es034362t.
Schwarz, J. P., et al. (2006), Single-particle measurements of midlatitude black carbon and light-scattering aerosols from the boundary layer to the lower stratosphere, *J. Geophys. Res.*, *111*, D16207, doi:10.1029/2006JD007076.
Schwarz, J. P., et al. (2008), Coatings and their enhancement of black-carbon light absorption in the tropical atmosphere, *J. Geophys. Res.*, *113*, D03203, doi:10.1029/2007JD009042.
Seinfeld, J. H., and S. N. Pandis (2006), *Atmospheric Chemistry and Physics: From Air Pollution to Climate Change*, Wiley-Intersci., Hoboken, N. J.
Stier, P., J. H. Seinfeld, S. Kinne, J. Feichter, and O. Boucher (2006), Impact of nonabsorbing anthropogenic aerosols on clear-sky atmospheric absorption, *J. Geophys. Res.*, *111*, D18201, doi:10.1029/2006JD007147.
Stier, P., J. H. Seinfeld, S. Kinne, and O. Boucher (2007), Aerosol absorption and radiative forcing, *Atmos. Chem. Phys.*, *7*, 5237–5261.
Streets, D. G., et al. (2003), An inventory of gaseous and primary aerosol emissions in Asia in the year 2000, *J. Geophys. Res.*, *108*(D21), 8809, doi:10.1029/2002JD003093.
Tomikawa, Y., and K. Sato (2005), Design of the NIPR trajectory model, *Polar Meteorol. Glaciol.*, *19*, 120–137.
Uno, I., G. R. Carmichael, D. Streets, S. Satake, T. Takemura, J.-H. Woo, M. Uematsu, and S. Ohta (2003), Analysis of surface black carbon distributions during ACE-Asia using a regional-scale aerosol model, *J. Geophys. Res.*, *108*(D23), 8636, doi:10.1029/2002JD003252.
Wang, C. (2004), A model study on the climate impacts of black carbon aerosols, *J. Geophys. Res.*, *109*, D03106, doi:10.1029/2003JD004084.
Wehner, B., S. Philippin, A. Wiedensohler, V. Scheer, and R. Vogt (2004), Variability of non-volatile fractions of atmospheric aerosol particles with traffic influence, *Atmos. Environ.*, *38*, 6081–6090, doi:10.1016/j.atmosenv.2004.08.015.
Weingartner, E., H. Burtscher, and H. Baltensperger (1997), Hygroscopic properties of carbon and diesel soot particles, *Atmos. Environ.*, *31*, 2311–2327, doi:10.1016/S1352-2310(97)00023-X.
Wexler, A. S., F. W. Lurmann, and J. H. Seinfeld (1994), Modeling urban and regional aerosols, I. Model development, *Atmos. Environ.*, *28*, 531–546, doi:10.1016/1352-2310(94)90129-5.
Zhang, Y., and G. R. Carmichael (1999), The role of mineral aerosol in tropospheric chemistry in east Asia: A model study, *J. Appl. Meteorol.*, *38*, 353–366, doi:10.1175/1520-0450(1999)038<0353:TROMAI>2.0.CO;2.
Zhang, Y., and M. Z. Jacobson (2005), A comparative study of nucleation parameterizations for 3-D atmospheric models, paper presented at the 9th Atmospheric Sciences and Air Quality Conference, Am. Meteorol. Soc., San Francisco, Calif.
Zhang, Y., Y. Sunwoo, G. R. Carmichael, and V. Kotamarthi (1994), Photochemical oxidant processes in the presence of dust: An evaluation of the impact of dust on particulate nitrate and ozone formation, *J. Appl. Meteorol.*, *33*, 813–824, doi:10.1175/1520-0450(1994)033<0813:POPITP>2.0.CO;2.
Zhang, Y., B. Pun, K. Vijayaraghavan, S. Wu, C. Seigneur, S. N. Pandis, M. Z. Jacobson, A. Nenes, and J. H. Seinfeld (2004), Development and application of the Model of Aerosol Dynamics, Reaction, Ionization, and Dissolution (MADRID), *J. Geophys. Res.*, *109*, D01202, doi:10.1029/2003JD003501.
Zhang, Y., P. Liu, K. Wang, M. Z. Jacobson, P. Bhave, S.-C. Yu, S. Roselle, and K. Schere (2005), Predicting aerosol number and size distribution with CMAQ: Homogeneous nucleation algorithms and process analysis, paper presented at the 2005 Models-3 Workshop, Community Model. and Anal. Syst., Chapel Hill, N. C.

M. Koike, Department of Earth and Planetary Science, Graduate School of Science, University of Tokyo, Hongo 7-3-1, Bunkyo-ku, Tokyo, 113-0033, Japan.
Y. Kondo, N. Moteki, N. Oshima, and N. Takegawa, Research Center for Advanced Science and Technology, University of Tokyo, 4-6-1 Komaba, Meguro-ku, Tokyo, 153-8904, Japan. (oshima@atmos.rcast.u-tokyo.ac.jp)
Y. Miyazaki, Institute of Low Temperature Science, Hokkaido University, N19 W8, Kita-ku, Sapporo, 060-0819, Japan.
Y. Zhang, Department of Marine, Earth, and Atmospheric Sciences, North Carolina State University, 2800 Faucette Drive, Raleigh, NC 27695-8208, USA.